

TC-2015-196

Combined Author Comments

We are very grateful for the thoughtful comments by both reviewers. They helped considerably to improve our manuscript.

Below, please find the reviewer comments in serif font and our **replies in bold sanserif font**.

We use a ***bold sanserif italic font*** to identify new or changed text.

We applied few minor improfements to enhance the readability of the manuscript.

Please find all changes highlighted (~~old~~ and new) in the appended manuscript.

Reply to Comments by Anonymous Referee #1

This study represents a nice demonstration of the utility of air-borne hyperspectral measurements for inferring spatial distributions of important snow properties. As the authors note in their conclusions, previous studies utilizing AVIRIS data have mostly focused on algorithm development and demonstrations of feasibility, whereas this study goes a bit deeper to describe actual variability in snow properties determined from a series of flights over the Rockies and Sierra Nevada. Most of the analysis shows variability in snow properties with elevation, aspect, and seasonal progression that are to be expected from basic physical arguments. Other measurements, however, show less intuitive distributions, such as the *positive* correlation between snow grain size and elevation seen in the Rockies during June, as well as the decrease in spatial variability of snow albedo observed during progression of the melt season. Such findings are really only feasible with remote sensing measurements, thus demonstrating their value. The manuscript is well-written and logically organized. Below are a few general comments and several minor comments that should be addressed prior to publication in *The Cryosphere*. Overall, however, I find the study and manuscript to be in good shape.

Major comments:

Data presented in Figure 9, panel h (15 June, terrain aspect plot) appear to show no grain size measurements between roughly 500 and 550 μm , with many measurements bracketing either side of this range. Is this gap an artifact of the retrieval algorithm (e.g., coarse discretization)? The gap should be explained, in any case, as it does not appear to be natural.

This gap is indeed an artifact. It is caused by non-unique solutions of Equation 4 where retrievals between 540 and 570 μm are lumped together, leaving a gap in between those values. It appears to be a rare case where the modeled HDRF at this given solar geometry and terrain can fit the data for multiple snow grain sizes. This effect is accentuated by the plotting routine, which removes ‘outliers’ where less than 15 pixels were found with the same combination of X and Y values.

More work would be required to fully understand and overcome this artifact by improved inversion methods. However, given all of our snow grain size retrievals, we think that this a rare and isolated case. Further, we do not think this artifact affects any of our conclusions in this paper. We thus decided to add a short description to the caption of Figure 9: “*Note: A rare retrieval artifact is found on 15 June 2011, where Eq. 4 has no unique solution within a snow grain size range of 540 to 570 μm causing a gap in the corresponding plots.*”

Second, how exactly were surface slope and aspect determined? Were these determined exclusively from the (snow-free) DEMs, or were they determined directly from the AVIRIS measurements? The normal to the surface can obviously change with snow accumulation, as valleys are filled, snow drifting occurs, etc. If DEMs were used to determine slope and aspect, please elaborate on the magnitudes of error that could result from variable (or inaccurate) slope

and aspect. If they were determined from the AVIRIS measurements, please explain how.

As mentioned in Sect. 2.1 (page 3, lines 2-10), we use the DEM, slope, and aspect data from the AVIRIS data products (specifically from the *_ort_igm and the *_obs_ort files), which are based on the USGS NED 1 arc second (~30 m) and converted from the raw GPS ellipsoidal elevation to orthometric elevations via the use of the NGA EGM96 global geoid model. From this, we determine the slope and aspects using standard routines provided by the ENVI software package, which are based on the following reference: “Wood, Joseph The Geomorphological Characterization of Digital Elevation Models, Ph. D. Thesis, University of Leicester, Department of Geography, Leicester, UK, 1996.”

It is worth mentioning that the DEM in our previous study (Painter et al, 2013) was based on the very coarse GTOPO30, which indeed was source of errors. The quality and the spatial resolution of the DEM used in this study is much better. This greatly improves the determination of the pixels being in the shadow of the terrain. In fact, terrain shadows can make up to 10% of the snow covered area early in the observed season. ATCOR-4 (Richter and Schläpfer, 2014) is capable of deriving the HDRF within shadows (by neglecting the direct irradiance component), but we suspect that strong adjacency effects in snow covered mountain terrain induce large uncertainties. We therefore remove those pixels from our analysis as explained in Sect. 4.5 (page 10, line 25). In addition, we typically find a few pixels (less than about 0.1% of the snow pixels) very close to a crest affected by the DEM where image data are attributed to the wrong side of the crest. The affected retrievals are found to be clear outliers. We don't show these retrievals in the density plots due to our threshold requirement of 15 pixels retrieved within the same bin of the histogram (see also our reply above). Lastly, we don't have a snow-on surface model available for this study, as opposed to our work performed within NASA's Airborne Snow Observatory (ASO). We therefore have no choice but to ignore this effect. However, we expect this to be a small source of errors for a majority of pixels. It would be worthwhile to test this hypothesis using data from ASO for example.

We improved our manuscript in Sect. 2.1 by mentioning AVIRIS and in Sect. 4.5 by specifically mention the issues related to crests and to the use of a snow-off DEM. The second paragraph of Sect. 4.5 is now worded as follows: “*Additional error sources are related to terrain shadows and the digital elevation model (Sect. 4.5). Up to 10% of the snow pixels in the February data are in shadow due to the large solar zenith angle. Snow properties can be retrieved in shadows using the diffuse irradiance. However, we suspect that large uncertainties are introduced due to adjacency effects, which are difficult to model in snow covered mountains. We therefore remove retrievals in shadow areas from our analysis, except for the snow cover calculation. Pixels very close to a crest can be associated with the wrong mountainside, which causes retrieval outliers. We found only very few snow pixels affected by this artifact and they do not show up in the histogram*

plots (Figs. 8, 9, and 12-15) due to a threshold of 15 occurrences. Changes in slope and aspect of the surface due to snow accumulation are not taken into account in this study and further analysis would be required to quantify associated errors.”

The term "radiative forcing" is used frequently, and it eventually becomes clear that this refers to surface radiative forcing from light absorbing impurities, but in general "radiative forcing" is ambiguous. It could also apply, e.g., to grain size effects. At first reference (in the abstract), and perhaps throughout the paper, this should instead be referred to with something like 'impurity radiative forcing' or 'LAISI radiative forcing'. It should also be mentioned early that the reference plane for the forcing is the surface (rather than top-of-atmosphere or tropopause or aircraft altitude).

Our Abstract already introduces the term LAISI on page 1, line 4 and is using it on line 12 as follows: “radiative forcing by LAISI.” We think that the current Abstract sufficiently addresses this comment. In the Introduction, we generalized the term ‘radiative forcing’ to ‘radiative effects’ on page 2, line 10-11. LAISI is introduced again on page 2, line 16 and subsequently used on page 2, line 24 to clarify the term ‘radiative forcing’. We added a note of clarification at this point in the manuscript that we refer to the forcing at the snowpack’s surface.

Related to the point above, do the radiative forcings represent local noon values or daily averaged values (or something different)? Please clarify.

Our radiative forcing quantities are derived with the local instantaneous solar irradiance, i.e. the actual W/m² entering the snowpack’s surface. We added language addressing this on page 7, line 1 such that the full sentence starting on page 6, line 28 reads: “*This reduction of spectral snow albedo by LAISI is multiplied by the direct and diffuse instantaneous spectral solar irradiance entering the snow surface and integrated over the given spectrum, such that the the additional radiative flux into the snow pack is given by:*”

Minor comments:

p1,13: Please specify the time period over which albedo decreases from 0.7 to 0.5. Presumably this is during the ablation period, but the ablation timeframe for each location should also be mentioned in the abstract.

We now mention the location specific ablation period by changing page 1, line 8-9 to: “*Our results show a linearly decreasing snow cover during the ablation period in May and June in the Rocky Mountains and a snowfall driven change in snow*

cover in the Sierra Nevada between February and May.”

p2,13: More precisely, this is the radius of a sphere that has specific surface area of SSA. For a polydisperse size distribution of spheres with collective specific surface area of SSA, it is the effective radius of that distribution.

We added: “*or the effective radius of a grain size distribution corresponding to a specific surface area (SSA).*”

p3,25: Wording (run-on sentence).

A period was added.

p4,3: particular -> particularly

Corrected.

p4,6: "end year dust concentrations" - Are these concentrations at the top of the snow, or are they column-averaged concentrations? If the former, please specify the thickness of snow over which the concentrations apply.

We added “*in the top 30 cm of the snow column*” for clarification.

p4,13-16: Sentence structure problems.

We added a period and moved the reference to increase the readability.

p5,22: Why are ‘ \approx ’ symbols used? Which wavelengths were actually used to determine the NDSI? And, were single AVIRIS bands used, or were spectral averages taken over multiple bands? Please clarify.

We now report the actual central wavelength used.

p6,6-8 (equation 4): If the ice absorption feature is centered at $1.27\mu\text{m}$, why is the upper bound of the integral at precisely $1.27\mu\text{m}$? (i.e., why not integrate over the feature, rather than up to it?). Presumably this is explained in one of the cited publications, but a very brief explanation for this may be warranted here.

We indeed use only the first half (1.17-1.27 microns) of the feature to reduce the crosstalk from the liquid water absorption feature, which starts to dominate the signal at longer wavelengths in the presence of meltwater. We reworked the text in Sect. 3.3 to highlight this fact.

Equation 5: I would speculate that this equation occasionally produces an observed albedo larger than 1, especially outside of the 1.17-1.27 μ m grain size calibration window. Does this ever happen, and is it necessary to cap the albedo at 1?

Spectral HDRF^{obs} and HDRF^{mdl} values can certainly be larger than 1. However, the anisotropy factor (Albedo^{mdl}/HDRF^{mdl}) scales the directional values to the hemispherically integrated albedo values, which are smaller than 1 at all wavelengths. We only derive spectral Albedo values larger than 1 where HDRF^{obs} was significantly overestimated. This would happen often the snow pixels in shadows would be included in the retrieval (using the diffuse irradiance to calculate the HDRF^{obs} is not sufficient due the adjacency effects, which make the observed snow brighter than expected by the model). Since we remove the shadow area, we might get some too low albedo value where the shadow mask fails to flag a shadow. Nevertheless, we retrieve very few albedo values larger than 1 close to the ridge of a steep mountainside as explained above. If the actual image pixel was in forward scattering, but we assume backward scattering in our model, we do not compensate correctly with the anisotropy factor for the large HRDF^{obs}, which lead to an overestimation in the spectral Albedo^{obs}. However, these few false retrievals do not show up in our plots because they either fall beyond the max value of the color table or they are ignored in the 2D histograms thanks to application of a frequency threshold of 15.

Section 3.6 discussion: This is fine (and helpful), but it should be clarified (e.g., in section 1) that the optical grain radius used here is a sphere-equivalent optical radius.

We already have such a statement on page 2, line 8. We modified it slightly to include the fact that we assume spheres according to your suggestion.

p7,11: Again, is the radiative forcing uncertainty defined with respect to daily-mean forcing or local noon instantaneous forcing?

We addressed this point as stated above.

p8,3-7: Please rework this passage for grammar and clarity.

We reworded this paragraph substantially.

p9,11: "In general the albedo increase with elevation is more distinct at the Sierra Nevada study area than in the Rocky Mountain study area." - This is interesting. Do you have any hypotheses for why?

This is actually a mistake. We wanted to state this in reverse order. We conclude this by looking at an imaginary fitting line to the data in Figs 12 and 13. We think that this might be related to the terrain itself. We fixed this in the manuscript.

p9,24-25: Again, are these instantaneous RF values?

We addressed this point as stated above.

p10,1: "all of the dust" -> maybe "nearly all of the dust"?

We changed this.

p10,15: Are you arguing here that earlier melt out on the south-west face reduces the time over which forcing can operate, therefore leading to greater forcing on the south-east face? Please clarify the relationship being described between processes on the south-east and south-west slopes.

We simply mean that there is no snow left on south-west facing slopes. The few remaining patches on those slopes indicate much lower RF values. However, would there still be snow on this slopes, the RF would likely be equally large as on the south-east slopes. We add the following sentence for clarification: *"The relatively low radiative forcing values on south-west to north facing slopes are likely from remnant patches of relatively clean snow."*

p11,16: Please check the wording in this section.

We reworded this paragraph.

p11,19-20: "The observed snow grains in the near-surface layer can therefore be smaller under intense snowmelt." - This is quite interesting!

Yes, indeed!

Figure 6 caption: Following previous comments, please clarify the source and temporal averaging domain of this forcing.

We now say: “Same as Fig. 4 but for effective snow radiative forcing at the time of overflight.”

Reply to Comments by M. Dumont (Referee)

This paper presents a really interesting data set of snow properties (optical grain size, broadband albedo and radiative forcing due to impurities) retrieved from hyperspectral airborne data over two mountainous areas. The areas and the retrieval methods are first described. The authors then present the results in term of spatial and temporal variations of the above mentioned snow properties. Note that the retrieval method has been described and evaluated in a previous paper (Painter et al., 2013).

This study is well written and fits well with The Cryosphere scope. The data set provided by the authors is quite unique. The study demonstrates the benefits of using high resolution airborne optical data to study in detail temporal and spatial variations of snow properties. It offers a new insight for the study of snow properties variability avoiding the limitations of point measurements. I think however that several questions should be addressed before it can be published.

Main Comments

1/ My first main comment focused on the grain size retrieval accuracy in presence of liquid water. It is stated section 3.3 that the range of wavelengths used in the grain size retrieval is 1.17 to 1.27 μm allowing to reduce the “bias (induced) by liquid water” with reference to Painter et al., 2013. In Painter et al., 2013, it is on the contrary stated that the retrieval is done using 1.03 to 1.06 μm wavelengths (section 4.3) and that the “technique could be less sensitive to biases due to liquid water and water vapor”. It is also stated that this assumption is not based on field measurements. Are the range of wavelengths used similar in this study and in Painter et al., 2013 or not ? In my mind, the assumption concerning the limited impact of liquid water on the retrieval should be discussed and demonstrated in more depth.

We discuss this now in a bit more depth. See our reply to reviewer #1. Our retrievals technique, as well as the contact probe-based methods in the field, can use both, the 1.27 or the 1.03 micron ice absorption feature.

For example, considering figure 1 in Gallet et al., 2014a or Green et al., 2002, there are some differences between the ice and water refractive indices in the considered range of wavelengths. This can induce some errors on the grain size retrieval and should probably be included in the discussion. The algorithms developed in Green et al., 2002 can also probably be used to investigate in more detail the effect of liquid water of the grain size retrieval and also to identify on the AVIRIS data snow with liquid water. I think this point is really crucial to infer the uncertainty of grain size retrieval and to strengthen the discussion on the grain size spatial and temporal variations presented in this study.

Gallet, J.-C., Domine, F., and Dumont, M.: Measuring the specific surface area of wet snow using 1310 nm reflectance, The Cryosphere, 8, 1139-1148, doi:10.5194/tc-8- 1139-2014, 2014a.

Green, R. O., Dozier, J., Roberts, D., Painter, T. (2002). Spectral snow-reflectance models for grain-size and liquid-water fraction in melting snow for the solar-reflected spectrum. *Annals of Glaciology*, 34(1), 71-73.

Please see Fig. R1 below showing the spectral absorption of the three water phases. The use of the spectral range in our method is a compromise between using enough bands (enough signal) vs staying away from information coming from liquid or gaseous water. We completely agree with Dr. Dumont's comment, but we believe that this topic would deserve its own full paper. For this paper, we wanted to focus on the application of the described methods and specifically on the related results. We try to maintain this balance and would argue to postpone a more detailed discussion of the snow grain size retrieval algorithm to another dedicated paper. Moreover, all our experience using this algorithm in different spectral ranges with different bands and even different sensors indicate that the results remain qualitatively the same, while the absolute retrieved microns change. However, the absolute numbers in snow grain size are less relevant in this paper in respect to their relative distribution space and change over time.

Note that we already refer to Gallet et al, 2014 on page 7, line 15.

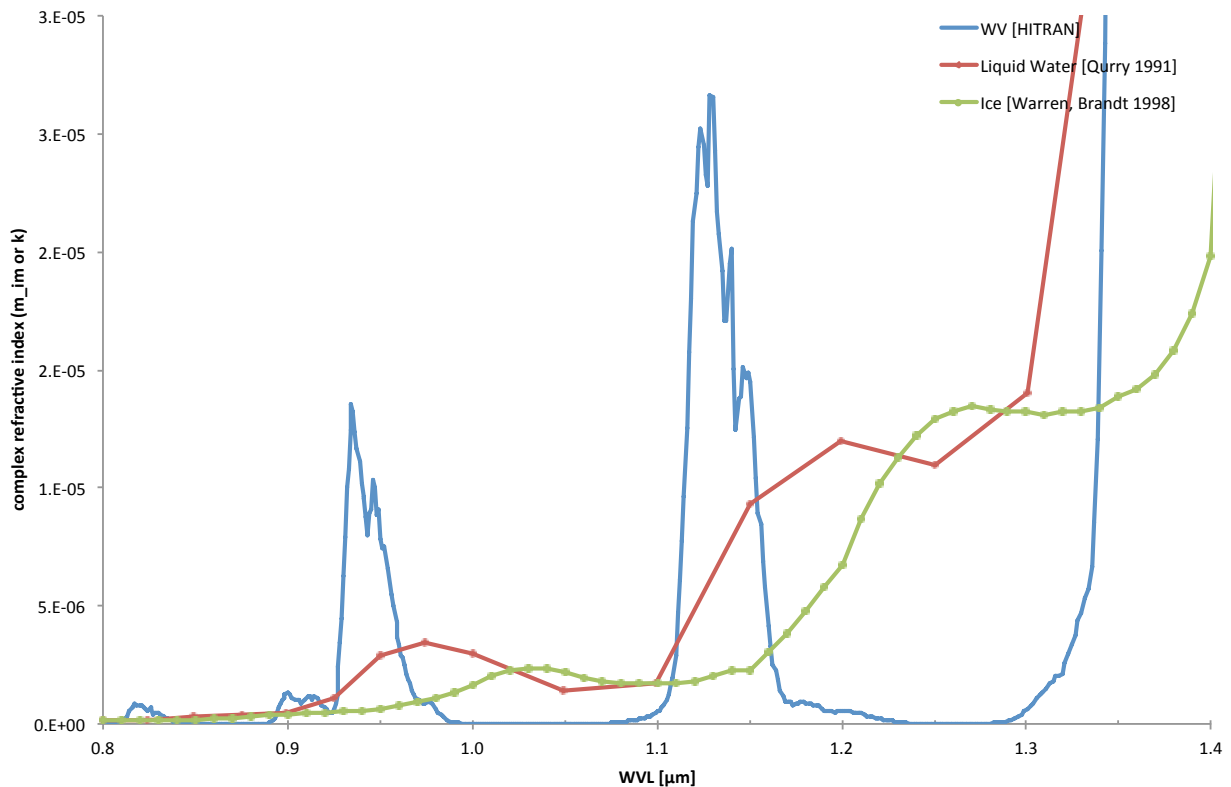


Figure R1. Refractive index (log scale) wrt wavelength of the three phases of water. The legend reports the data sources.

2/ The second main comment focuses on the grain size/elevation inverse relationship in case of large impurity load discussed in section 5. I think this is a really interesting finding and it would result in a negative feedback. It also has to be linked to other recent studies showing that light-absorbing impurity can reduce the density of melting snow (Meinander et al., 2014) or studying the effect of soot on anisotropy factor (Peltoniemi et al., 2015) However, the discussion should be strengthened to be more convincing. The first thing is that the mean decrease of grain size is roughly 50 μm (figures 7 and 9) which is close to the accuracy of the grain size retrieval method (the one given in Painter et al., 2013). Consequently, I think before discussing the possible physical causes of the grain size/elevation inverse relationship, the authors should probably discuss the significance of the grain size decrease relatively to differences sources of errors. There are several sources of errors that might have to be taken into consideration e.g. : a/ grain size retrieval accuracy in presence of liquid water (see my previous comment) b/ the fact that as stated by the authors the surface roughness is high. Consequently the HDRF derived from spherical model are probably more anisotropic than the natural surface inducing a larger error on the grain size for the rough surface than for flat one. c/ Peltoniemi et al., 2015 (see full reference below) also demonstrated that under large impurity load, the impurity sank in the snow and largely modify the HDRF . . . this also leads to an error in the grain size retrieval. d/ Finally, as discussed in Skiles PhD thesis (e.g. chapter 3, figure 1), it is possible that for really high impurity content, the snow reflectance is more dust-like than snow-like in the IR (and then higher in the NIR not due to snow grain size but to impurity particles). This effect seems to be overestimated by SNICAR (compared to field measurements) but it can still affect the grain size retrieval and results artificially smaller grain size.

Lastly, the processes leading to a decrease of snow grain size could probably further discussed : the presence of a large content of impurity largely modifies (and shortens) the light penetration depth so that the energy is absorbed closer to the surface. The temperature profile and the heat and vapour transfer are consequently modified leading to modified metamorphism. Note that the formation of sublimation crystals has also been discussed in Antarctica (Gallet et al., 2014b, see full reference below).

Meinander, O., Kontu, A., Virkkula, A., Arola, A., Backman, L., Dagsson- Waldhauserová, P., Järvinen, O., Manninen, T., Svensson, J., de Leeuw, G., and Lep- pärinta, M.: Brief communication: Light-absorbing impurities can reduce the density of melting snow, The Cryosphere, 8, 991-995, doi:10.5194/tc-8-991-2014, 2014.

Peltoniemi, J. I., Gritsevich, M., Hakala, T., Dagsson-Waldhauserová, P., Arnalds, Ó., Anttila, K., Hannula, H.-R., Kivekäs, N., Lihavainen, H., Meinander, O., Svens- son, J., Virkkula, A., and de Leeuw, G.: Soot on Snow experiment: bidirectional re- flectance factor measurements of contaminated snow, The Cryosphere, 9, 2323-2337, doi:10.5194/tc-9-2323-2015, 2015.

Gallet, J.-C., Domine, F., Savarino, J., Dumont, M., and Brun, E.: The growth of sub- limation crystals and surface hoar on the Antarctic plateau, The Cryosphere, 8, 1205- 1215, doi:10.5194/tc-8-1205-2014, 2014b.

It is true that absolute retrieval accuracy of snow grain size might be in the order

of the changes observed in late June 2011, however, we believe that the observed trend is due to physical processes and not retrieval error. In other words, we are confident in tracing trends in snow grain sizes across a single image and from observation to observation. Especially given that the inverse relationship with elevation and grain size has been observed in imagery from other years, and a decrease in optical grain size was observed in the field in presence of heavy dust loading/absence of new snowfall.

We would like to note that the surface roughness mentioned in the paper was observed by co-author Skiles in the field as the upper layers of snowpack transitioned from relatively clean to dirty snow over the course of a few days in 2013. High resolution ground observations like these were not available for 2011 when the over flights presented here were taking place, and therefore we cannot say whether or not there was surface roughness during time of acquisition. We do recognize that surface roughness can affect the bidirectional reflectance distribution function of snow. That being said, we note here (from Painter et al., 2003) ‘that Warren et al. (1998) found the effect of sastrugi negligible for near-nadir views. Moreover, they found that sastrugi have little effect on the BRDF for view angles less than 30° in the principal plane and for view zenith angles less than 50° for $\lambda=0.9 \mu\text{m}$ and solar zenith angle $\theta_0=67^\circ$, an effect that should be even smaller for smaller zenith angles.’ Therefore, the assumption that surface roughness has a negligible impact on snow bidirectional reflectance should be valid for the AVIRIS scenes examined here.

We agree that this is an interesting finding, and deserves attention, but believe a more extended discussion on the processes leading to a decrease of snow grain size is outside the scope of this paper, which focuses on ability to monitor snow cover trends using imaging spectroscopy. There are two papers that are currently in preparation by co-author Skiles, based on her dissertation work, that address this process in much more detail, including the field observations and assessing the impact of increasing dust concentrations/water content on NIR absorption and grain size retrieval.

We address this in the manuscript by modifying the second sentence in the paragraph that discusses the grainsize inversion such that this paragraph becomes: *“Second, when there is an actual inversion of grain sizes with elevation, we suggest this is accounted for by rapid melt induced by high impurity content at the surface. Although the change in grain size is on the order of the uncertainty in grain size retrieval, it is not the absolute values that are important but rather the trend. A decrease in surface grainsize in the presence of high impurity content was also observed in the daily field observations in 2013 by Skiles (2014), when the dust layers coalesced at the surface and skies were clear both grain sizes and density in the surface layers decreased and surface roughness increased.”*

3/ The third main comment focuses on the way the data are presented in Figures 8 and 9 with respect and elevation. I think the figures really nicely described the variations of the snow parameters with respect to topographic parameters. However, especially at the end of the season, when the snowpack remains mainly on shaded slopes this way to present the data could induce a bias in the interpretation. In other words, I mean that it is, for example, not straightforward from Figure 9, 3rd row that the inverse grain/size elevation relationship is not a bias due to uneven distribution of snow cover with elevation and aspect. Consequently, my suggestion would be to plot the value of mean grain size (colour) as a function of aspect (x-axis) and elevation (y-axis) with a representation of the RMSE or the number of points in each topographic class (transparency or size of the dots).

The sun is rising much higher (decreasing solar zenith angles) later in the ablation period where we observe the inverse relationship between grain size and elevation. In June, there are almost no shadows left at the time of observation, which typically is close to the local solar noon. We therefore do not think the shadows would introduce a significant bias or even have an impact on our conclusions.

We appreciate the suggested plot, which would bring the elevation and the terrain dependence into one single panel. We experimented extensively with this and other types of plots and we found the current plot to be most effective in illustrating the dependencies. The main reason for that is that the current plots show the density or number of occurrences by using 2D histograms. This density carries additional information, which is very helpful in the visual interpretation of the results. With the suggested scatterplot, however, the reader has to imagine the clustering, which is not easy in the ablation cases where we see a low dependency of snow grain size with respect to the terrain (see Fig. R2). We also created polar plots to simplify the interpretation of the terrain aspect, but we were also not happy with this. After careful consideration, we therefore believe that our current plots are optimal for the abovementioned reasons.

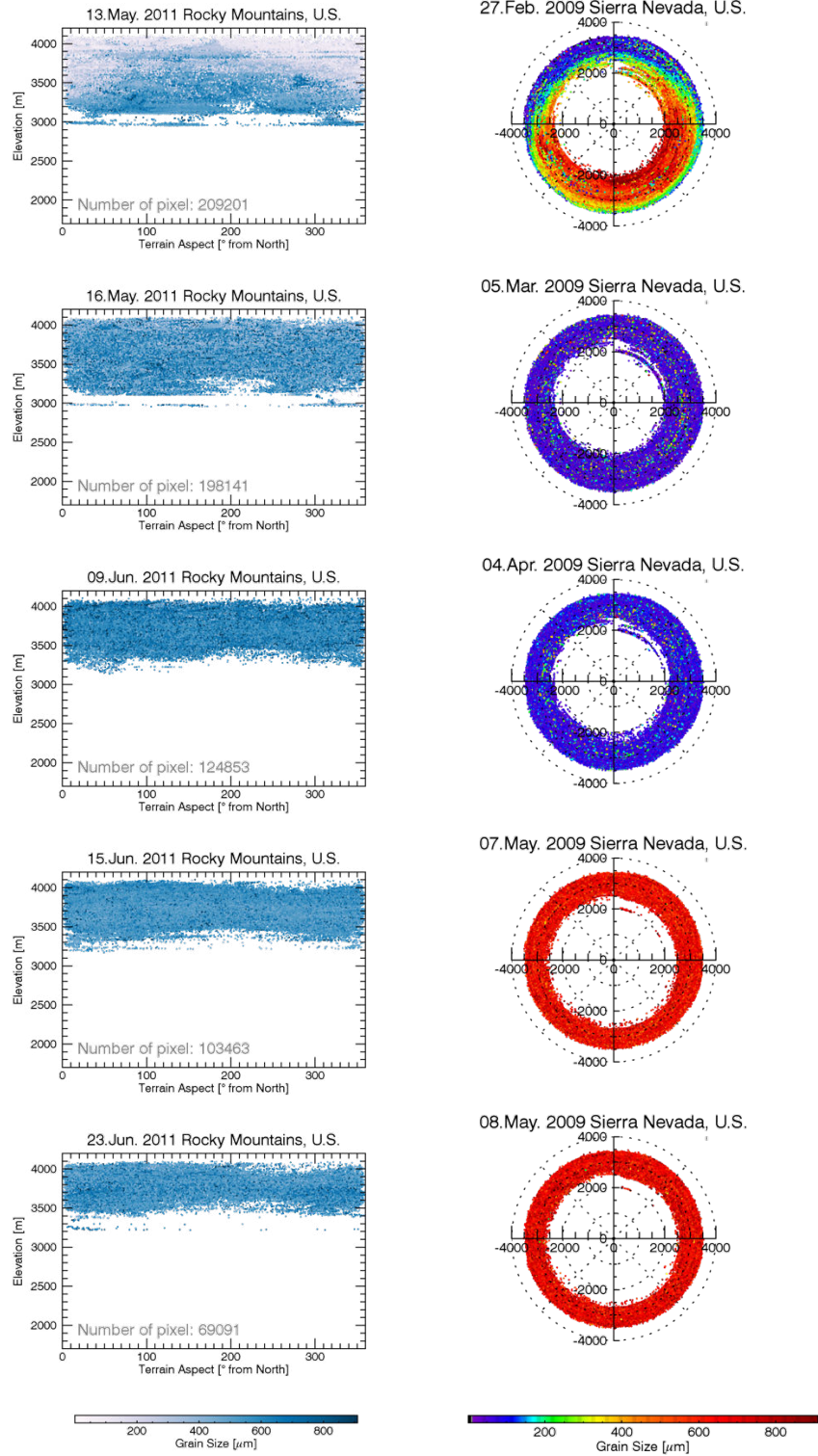


Figure R1. Experimental plots addressing Dr. Dumont's suggestion (3). North is up in the polar plots and the elevation is plotted as radius.

4/ The last main comment focuses on the uncertainties analysis provided in the paper. Though I perfectly agree that uncertainty analysis is not the main aim of the paper, I think that a deeper analysis of the errors could help to strengthen the conclusions of the paper as I explained in the previous comments. The authors refers to the uncertainties of the retrieval method provided in Painter et al., 2013 as being 25um for grain size, 0.0001 (there must be a typo there) for snow albedo and 4 Wm² for radiative forcing. In Painter et al. 2013, the uncertainties given for albedo is 0.001-0.004 (based on two measurements only. . .), 2.1 +-5.1 Wm² for radiative forcing, and the uncertainty of the grain size retrieval is an assumption. In Painter et al., 2013, only one date was available for AVIRIS data but with all the dates used in the study, I am wondering if the uncertainty data could used more broadband albedo measurements to strengthen the uncertainty analysis. Section 4.5. presents really interesting results regarding the comparison of two images acquired only one day apart from each other but it would worth a more detailed analysis. Are the given values mean values ? What are the spreads of the difference ? In my mind, the uncertainty analysis should be more careful, describing which values are assumed, what is the significance of the different values (how many measurements are used to derive the uncertainty). . .

We realize that having two sections with error/accuracy discussions might be confusing. We therefore decided to merge the two sections into Sect. 4.5. We have completely rewritten this section and we now account and correct for all of the points raised by this reviewer's comment.

Specific Comments

Page 2, line 13 : Maybe the authors can be a bit more explicit why the SSA /optical grain radius relationship is not a strict equality.

We believe that the this is covered by the two references and further discussion is out of scope for this paper.

Section 3.3 . The modeled HDRF must account for the diffuse to total incoming irradiance ratio. Therefore it could worth explaining how this ratio is calculated. For this section, please see also my main comment 1/.

The ratio is calculated from diffuse and total incoming irradiance, which are both produced by ATCOR-4 (the authors specifically requested this capability to simplify automated processing of imaging spectrometer products from the Airborne Snow Observatory). We add language to specifically state this in Sect. 3.4 where we introduce the (total) irradiance term.

Page 7, Equation 7 : If c is meant to account for imperfect terrain corrections, c probably also have a second order dependency to wavelength. This could be maybe detailed in the paper.

Yes, c is some sort of calibration to remove imperfections, mainly induced by the terrain. We reason why we choose 1.08 microns is already described on page 7, line 4 and 5.

Page 7, line 13 : *This assumption becomes more valid with grain growth associated with evolving metamorphism and rounding of the snow crystals.* Rounded forms do not necessarily means perfect spheres, and spheroids optical properties might significantly differ from spheres optical properties (e.g. Libois et al., 2013, full ref below, fig1). The differences between spheres and spheroids optical properties might even be larger that the ones between spheres and other snow crystals optical properties. Consequently, in my mind, this sentence should be either removed or further justified.

Libois, Q., Picard, G., France, J. L., Arnaud, L., Dumont, M., Carmagnola, C. M., and King, M. D.: Influence of grain shape on light penetration in snow, The Cryosphere, 7, 1803-1818, doi:10.5194/tc-7-1803-2013, 2013.

We removed this sentence.

Page 8, lines 9-13 : The mean broadband albedo varies not only with the snow properties but also with the illumination geometry and consequently the date and time of acquisition. This should probably be discussed while presenting the results of Figure 7.

Albedo is higher when the sun is closer to the horizon, but the difference is small relative to impact of grain size/impurity content. We added the following text to the first paragraph of Sect. 4.5: “*While inherent snow albedo is controlled by grain size and impurity content over the course of a day, the solar zenith angle, cloud cover, and topography also act to influence albedo and net solar radiation (Warren, 1982). For our acquisitions, we account for local illumination and view geometries in the albedo retrievals (Eq. 2 and 5).*”

Section 4.3. Same comment as above. Snow albedo depends not only on the snow properties but also on the illumination conditions. This has, in my mind, to be taken into account in the discussion regarding the spatial variations of albedo.

Local illumination and view geometries are accounted for in our algorithms (See Eq. 2).

Minor Comments

Page 2, line 16 : Changes in surface roughness also cause changes in snow albedo

We added surface roughness.

Page 4, line 22 : “retrieved columnar water vapor”, maybe the authors could explain how, and from which data and add a reference.

We mention ATCOR-4 here and added the corresponding reference.

Page 8, line 18 : Surface snow grain size can also be affected by wind effects.

We added the wind effects.

Case study of spatial and temporal variability of snow cover, grain size, albedo and radiative forcing in the Sierra Nevada and Rocky Mountain snowpack derived from imaging spectroscopy

F. C. Seidel¹, K. Rittger², S. M. Skiles¹, T. H. Painter¹, and N. P. Molotch^{3,1}

¹Jet Propulsion Laboratory / California Institute of Technology, Pasadena CA, USA

²National Snow and Ice Data Center, University of Colorado, Boulder CO, USA

³Department of Geography, Institute of Arctic and Alpine Research, University of Colorado, Boulder CO, USA

Correspondence to: F. C. Seidel (Felix.C.Seidel@gmail.com)

Abstract. Quantifying the spatial distribution and temporal change in mountain snow cover, microphysical and optical properties is important to improve our understanding of the local energy balance and the related snowmelt and hydrological processes. In this paper, we analyze changes of snow cover, optical-equivalent snow grain size (radius), snow albedo, and radiative forcing by Light Absorbing Impurities in Snow and Ice (LAISI) with respect to terrain elevation and aspect at multiple dates during the snowmelt period. These snow properties are derived from Airborne Visible/Infrared Imaging Spectrometer (AVIRIS) data from 2009 ~~of the maritime snowpack~~ in California's Sierra Nevada and from 2011 ~~of the continental snowpack~~ in Colorado's Rocky Mountains, USA.

Our results show a linearly decreasing snow cover during the ablation ~~season in period in May and June in~~ the Rocky Mountains and a snowfall driven change in snow cover in the Sierra Nevada between February and May. At the same time, the snow grain size is increasing primarily at higher elevations and north facing slopes from 200 microns to 800 microns on average. We find that intense snowmelt renders the mean grain size almost invariant with respect to elevation and aspect. Our results confirm the inverse relationship between snow albedo and grain size, as well as between snow albedo and radiative forcing by LAISI. At both study sites, the mean snow albedo value decreases from approximately 0.7 to 0.5 during the ablation period. The mean snow grain size increased from approximately 150 to 650 microns. The mean radiative forcing increases from ~~20 W m⁻² up to~~ 200 W m⁻² 20 W m⁻² up to 200 W m⁻² during the ablation period. The variability of snow albedo and grain size decreases in general with the progression of the ablation period. The spatial variability of the snow albedo and grain size decreases through the melt season while the spatial variability of radiative forcing remains constant.

1 Introduction

Snow is important to the ~~hydro-and-biosphere, to~~ climate and hydrology of mountain and arctic ~~regional climates~~ regions, as well as to water resources management ~~as a natural water storage~~. Snow influences the Earth's energy balance through its strong albedo feedback. Changes to the snow cover extent, snow albedo and snow water equivalent, therefore have direct impacts on the environment, water availability and economics. In the Western United States, seasonal snowmelt provides more than 70%

of water supply. The Sierra Nevada in California and the Rocky Mountains in Colorado are examples of two mountain ranges where reservoirs store snowmelt for use in late spring and throughout the summer and early fall when precipitation is less frequent. As such, these regions are of great interest to snow research and water management (Bales et al., 2006).

Snowmelt in mid-latitude mountains is largely dominated by the absorbed solar radiation (Marks and Dozier, 1992; Oerle-
5 mans, 2000; Painter et al., 2007a). The net shortwave radiation is a function of the solar zenith, cloud cover, aerosol attenuation,
surface albedo, as well as ~~terrain elevation~~, slope and aspect of the terrain. The solar irradiance at the surface is highly variable
in mountainous areas mainly due to the complex terrain, cloud cover, and vegetation above the snow surface (Link and Marks,
1999; Garen and Marks, 2005). Besides snowmelt, snowfall impacts snowpack properties very rapidly and thus, it is important
to capture temporal changes in addition to spatial patterns. For example, Molotch et al. (2004) showed that spatially-distributed
10 snowmelt models benefit significantly from incorporating snow albedo estimates derived from AVIRIS data instead of using
empirical basin-wide snow albedo assumptions.

Snow microstructure is a ~~key~~ indicator of physical processes occurring in a snowpack. Snow grain size is generally used
as a proxy for the microstructure due to the lack of a direct measurement technique. Throughout this paper, we refer to the
optical-equivalent snow grain radius (r), or simply snow grain size for brevity. It can be estimated with handheld spectroscopy
15 instruments (Painter et al., 2007b; Skiles, 2014) as well as airborne imaging spectroscopy (Nolin and Dozier, 2000; Painter
et al., 2003, 2013). The former can be used to resolve the vertical distribution of snow grain sizes within a snowpack, and the
latter is very useful to resolve the spatial and temporal distribution of not only snow grain size but also albedo and radiative
~~foreing effects~~ on scales useful for snow hydrology. It should be noted that r should not be directly compared with the snow
grain size derived using other measurement techniques, such as for example the traditional visually estimated snow grain size
20 or the effective radius of a grain size distribution corresponding to a specific surface area (SSA). Gallet et al. (2009) and
Leppänen et al. (2015) suggest a conversion of $r = 3/(\rho_{ice} SSA)$, where ρ_{ice} is the density of ice (~~917 kg m⁻²~~ 917 kg m⁻²).
An optical-equivalent snow grain radius of ~~100 μ m and 650 μ m~~ 100 μ m and 650 μ m corresponds therefore to a SSA of
~~33 m² kg⁻¹ and 5 m² kg⁻¹~~ 33 m² kg⁻¹ and 5 m² kg⁻¹, respectively.

Snow albedo is a key parameter to the Earth's energy balance. The snow albedo feedback mechanism has a strong impact
25 on climate on all temporal and spatial scales. In particular, snow albedo is a dominant driver of snowmelt, ecohydrological
processes, as well as water supplies. Snow albedo is mainly changed by snowfall, metamorphism, surface roughness, and light
absorbing impurities in snow and ice (LAISI). While fresh snow with small grains has a high albedo value, aged snow has a
lower albedo value in conjunction with snow grain size growth and change in optical path length. LAISI, such as black carbon,
dust, and tree litter have the most profound impacts on snow albedo (Warren and Wiscombe, 1980; Qian et al., 2015).

This 'darkening' of snow increases the absorption of solar ~~irradiation~~ irradiance, which reduces the cold content of the
30 snowpack or enhances snowmelt if its temperature is at 0°C. The related consequences of LAISI to snow hydrological and
climatological processes became more evident by the work of Ramanathan et al. (2007); Painter et al. (2007a); Qian et al.
(2009); Flanner et al. (2009); Painter et al. (2010, 2012b) and others, and novel remote sensing algorithms were developed by
Painter et al. (2012a, 2013) to retrieve the radiative forcing by LAISI at the snow surface.

The ~~combination of~~ objective of this research is to use imaging spectroscopy to identify the spatio-temporal distribution of quantitative snow properties at study sites in the Sierra Nevada and Rocky Mountains. The Airborne/Visible Infrared Imaging Spectrometer (AVIRIS) data ~~(and the study sites are described below in Sect. 2.4) with our algorithms (2 followed by our retrieval algorithms in Sect. 3) allow us to address the temporal variation and spatial distribution of snow properties in two~~ partial hydrological catchment areas located in the Rocky Mountains, Colorado and the Sierra Nevada, California, USA (Sect. 2.2) as-. Results are presented in Sect. 4 ~~and with the most interesting findings~~ discussed in Sect. 5 ~~about the relationship between elevation and grain size for melting snow.~~

~~2 California and Colorado study area and data description~~

~~In the Western United States, seasonal snowmelt provides more than 70% of water supply. The Sierra Nevada in California and the Rocky Mountains in Colorado are examples of two mountain ranges where reservoirs store snowmelt for use in late spring and throughout the summer and early fall when precipitation is less frequent. As such, these regions are of great interest to snow research and water management and we analyze data in each.~~

2 California and Colorado study areas and data description

2.1 Terrain

We use the United States Geological Survey National Elevation Dataset (NED) with one arc second spatial resolution (roughly 30 m) ~~as provided by the AVIRIS data product.~~ A hill shaded version is used as background to Fig. 1. The Sierra Nevada study region covers a larger distribution of elevations with a vertical range of 2400 m while the Colorado study area has a vertical range of only 1200 m (Fig. 2). The Colorado study area reaches higher elevations with a maximum at 4111 m, while the maximum elevation in the California study area is only 3533 m. The mean elevation is over 1000 m higher in the Colorado study area (Table 1). The Kaweah and Kings River basins in Sierra Nevada study area drain to the West as seen in the distribution of aspects with a peak around 270° in Fig. 2. The Uncompahgre River basin drains to the North hence the lower percentage of 180° slopes. A larger proportion of the Uncompahgre slopes face East and West draining toward the center of the basin explaining the larger percentage of the basin with aspects of 90° and 270° .

2.2 Snow hydrology

In the Sierra Nevada of California, the study area covers part of the Kings and Kaweah river basins. In the Rocky Mountains of Colorado, the study area covers the Senator Beck drainage, which is part of the Uncompahgre watershed (Skiles et al., 2012; Painter et al., 2012b, 2013). The Kings and Kaweah have maritime snowpacks (typically warmer and deeper) while the Uncompahgre has a continental mountain ~~or Alpine~~ snowpack (typically colder and more shallow) (Sturm et al., 1995), allowing us to test our algorithms in different snow regimes.

We use snow pillow data of snow water equivalent (SWE) at high and low elevation as a proxy for snow accumulation or snowmelt as shown in Fig. 3. We choose the Big Meadow (36.72N, 118.84W, 2300 m., Kings) and the Farewell Gap (36.41N 118.58W, 2900 m., Kaweah) stations to represent the California study area. For Colorado, we choose the Idarado (37.93N, 107.68W, 3000 m., Uncompahgre) and the Red Mountain Pass (37.90N, 107.72W, 3400 m., Uncompahgre) SNOTEL stations.

5 Based on those SWE data, 2009 was an average year in the Sierra Nevada, and 2011 was an above average year in the Rocky Mountains. Peak SWE and length of the ablation ~~season-period~~ were fairly similar at the two high elevations stations in each area, but separated by a month. At Farewell Gap SWE peaked ca. 80 cm on 17 April 2009 and snow melt out occurred on 19 May 2009. At Red Mountain Pass SWE peaked at ca. 85 cm on 25 May 2011 and melt out occurred on 20 June 2011.

~~This is not to say that the two study areas are similar, in addition to~~ In addition to regional and interannual variability, there was some distinct differences in melt patterns. In Kings/Kaweah multiple snowfall events refreshed the snow surface over the period of flight, delaying the main snowmelt pulse until just prior to snow melt out. In the Uncompahgre melt initiated just after peak SWE and steadily increased over the ablation period, with the exception of a minor snowfall event at the end of May. While the measurement sites may not be wholly representative of the two study areas, they are helpful in interpreting some of the spatial and temporal variability ~~exhibited in the acquisitions, observed and~~ discussed in Sect. 4.

15 2.3 Dust concentrations in snow

~~The~~ Senator Beck Basin is a research catchment established to monitor the hydrological impacts of regularly observed episodic events of dust deposition on snow in the Upper Colorado River Basin (Painter et al., 2012b). Dust is ~~particular-particularly~~ effective at altering ~~the~~ snow energy balance in this region because the majority of mass is deposited in the spring coinciding with snowmelt onset (80% of ~~dust deposition~~ events occur March-May), and additionally, dust is inefficiently scavenged by melt water and layers coalesce at the surface as snow melts, compounding albedo decay. Over the ten year record (2005-2015) ~~end-year dust concentrations~~ ~~dust concentrations toward the end of the snow season~~ have ranged from ~~0.83 to 4.83 mg g⁻¹~~ ~~0.8 to 4.8 mg g⁻¹ in the top 30 cm of the snow column~~, and exhibit a bimodal distribution, with about ~~1 mg g⁻¹~~ ~~1 mg g⁻¹~~ in lesser dust years and over ~~4 mg g⁻¹~~ ~~4 mg g⁻¹~~ in extreme dust years (Skiles et al., 2015). There were nine observed dust events in 2011 after March 1st and the end of year dust concentration was ~~1.3 mg g⁻¹~~ ~~1.3 mg g⁻¹~~, making it a lesser dust year. Black carbon has only been monitored across the 2013 ablation ~~season-period~~, and concentrations were so low (~~1 to 20 ng g⁻¹~~ ~~1 to 20 ng g⁻¹~~) that it was concluded that its contribution to radiative forcing by LAISI in this region is negligible in the presence of such heavy dust loading (Skiles, 2014).

Unfortunately, ~~there is not a similar data set for any basin~~ ~~similar dust deposition data do not exist~~ in the Sierra Nevada, but given the predominant wind patterns and location of dust emission sources in the western US, ~~we would not expect as great of~~ ~~dust loading there~~ ~~dust deposition is expected to be relatively low~~. There was a study conducted in the eastern Sierra Nevada in 2009 by Sterle et al. (2013) which found surface black carbon concentrations of ~~1 to 75 ng g⁻¹~~ ~~1 to 75 ng g⁻¹~~ and dust concentrations of ~~1 to 44 μg g⁻¹~~ ~~1 to 44 μg g⁻¹~~ over the ablation ~~season, despite-period~~. ~~Despite~~ the lower concentrations sampled in the Sierra Nevada relative to the Rocky Mountains, this study also concluded that dust dominated the radiative forcing (Sterle et al., 2013).

2.4 Imaging spectroscopy data

Results provided in this paper were derived from georeferenced at-sensor radiances acquired by the NASA/JPL Airborne Visible/Infrared Imaging Spectrometer (AVIRIS) flown on NASA's ER-2 high altitude aircraft and on a Twin Otter aircraft. Table 2 shows specific information for each flight line including aircraft altitude and heading, terrain elevation, pixel size, solar geometry, as well as ~~retrieved~~ columnar water vapor retrieved by using the Atmospheric / Topographic Correction for Airborne Imagery (ATCOR-4) software (Richter and Schläpfer, 2014). The pixel size is directly related to the terrain height and the aircraft altitude, which varied significantly between acquisition dates. We therefore resampled the AVIRIS data to the common coarsest resolutions of ~~14.5 m and 13.8 m~~ 14.5 m and 13.8 m for California and Colorado, respectively. For each acquisition date, the images are mosaicked and cropped to their common area (~~252 km²~~ 252 km² in California and ~~54.7 km²~~ 54.7 km² in Colorado). This enables inter-comparisons between acquisition dates at the pixel-level. Figure 1 shows the outline of each flight line overlaid on the terrain for each study area (intersection of all flight dates) as a hatched line. ~~The 27 February 2009 and 13 May 2011 lines for California and Colorado respectively lie directly on the study area because they covered the smallest area.~~

3 Remote sensing retrievals of quantitative snow properties

The quantitative snow properties shown and analyzed in this paper are extracted from imaging spectrometer data using retrievals based on a legacy of algorithms by e.g. Nolin and Dozier (2000); Painter et al. (2001, 2003); Painter and Dozier (2004); Green et al. (2006); Dozier et al. (2009). Our retrieval algorithms are described in details in Painter et al. (2013) and summarized in this section for reference.

3.1 Directional reflectance

Reflected and scattered solar radiation are observed by the airborne spectrometer and transformed into calibrated radiance for each wavelength band λ_i , based on band-wise calibration.

The retrieval of surface properties requires that we convert the measured radiance first to reflectance at the sensor level R_{sensor}^{obs} and then to surface directional reflectance by compensation of atmospheric scattering and absorption. We use the ~~Atmospheric / Topographic Correction for Airborne Imagery (ATCOR-4) (Richter and Schläpfer, 2014) software~~ software (Richter and Schläpfer, 2014) to model the reflectance of the atmosphere at the sensor level R_{atm}^{mdl} , the total transmittance $T^{\uparrow, mdl}$, and the spherical albedo at the surface level S_{sfc}^{mdl} to derive the spectral Hemispherical-Directional Reflectance Factor at the surface level from R_{sensor}^{obs} (Schaepman-Strub et al., 2006):

$$HDRF_{sfc}^{obs} = \frac{R_{sensor}^{obs} - R_{atm}^{mdl}}{T^{\uparrow, mdl} + S_{sfc}^{mdl} (R_{sensor}^{obs} - R_{atm}^{mdl})}. \quad (1)$$

Note that the rugged terrain in both study areas (see Sect. 2) requires us to account for the local solar and viewing angles at each terrain facet. Local zenith angles are derived by:

$$\theta'_{[\odot, v]} = \arccos \left(\cos \theta_{[\odot, v]} \cdot \cos slp + \sin \theta_{[\odot, v]} \cdot \sin slp \cdot \cos \varphi' \right), \quad (2)$$

where $\varphi' = \varphi - asp$, slp and asp denote the terrain's slope and aspect, respectively. All angles are defined in degrees. Although the following geometries are locally defined with respect to the terrain, we omit its notation for readability. Note that we mask pixels affected by terrain shadows in our retrievals, except for the snow cover determination.

3.2 Snow cover

A byproduct derived from $HDRF_{sfc}^{obs}$ is the snow cover map. We apply the normalized difference snow index (NDSI):

$$NDSI \equiv \frac{HDRF_{sfc}^{obs}(\lambda_{VIS}) - HDRF_{sfc}^{obs}(\lambda_{SWIR})}{HDRF_{sfc}^{obs}(\lambda_{VIS}) + HDRF_{sfc}^{obs}(\lambda_{SWIR})}, \quad (3)$$

where $\lambda_{VIS} \approx 0.6 \mu\text{m}$ and $\lambda_{SWIR} \approx 1.5 \mu\text{m}$ ~~$\lambda_{VIS} = 0.668 \mu\text{m}$ and $\lambda_{SWIR} = 1.502 \mu\text{m}$~~ (Dozier and Marks, 1987; Dozier, 1989; Hall et al., 2002). To mask partially covered snow pixels, we empirically determined NDSI thresholds of 0.90 for the Sierra Nevada and 0.93 for the Rocky Mountains by visual interpretation with the corresponding true-color images. The high spatial resolution of the AVIRIS imagery (see Table 2) allows the use of this simple technique without rejecting too many pixels. The multiplication of the number of remaining snow pixels by the pixel size yields the approximate (low-biased) snow covered area. We sum the snow covered area and normalize it with the study area to report the approximate percent snow cover.

3.3 Snow grain size

The optical-equivalent snow grain size, reported here as radius r , is an important snow property and prerequisite for the snow albedo retrieval.

Based on Nolin and Dozier (2000), we derive the snow grain size by searching for the best fit between the observed $HDRF_{snow}^{obs}$ and modeled $HDRF_{snow}^{mdl}$ snow spectra with the minimum sum of absolute differences:

$$r : \left[\min_{i=1.17 \mu\text{m}}^{1.27 \mu\text{m}} \left| HDRF_{snow}^{mdl}(\theta_{\odot}, \theta_v, \varphi; r; \lambda_i) - HDRF_{snow}^{obs}(\theta_{\odot}, \theta_v, \varphi; \lambda_i) \right| \right]. \quad (4)$$

We assume to observe a single layer with ~~a homogeneous snow grain size~~ homogeneous spherical snow grains. Using the ice absorption feature centered around ~~1.27 μm~~ 1.27 μm allows us to probe the uppermost layer in the snowpack with a depth in the order of ~~1 cm~~ 1 cm (Nolin and Dozier, 2000; Gallet et al., 2009). $HDRF_{snow}^{mdl}$ is modeled using the radiative transfer code DISORT (Stamnes et al., 1988; Painter et al., 2003). The two spectra are matched at the corresponding solar and viewing geometry for each pixel in the terrain. The fit is performed at AVIRIS band numbers 86 to 99, which correspond to the wavelength interval $\lambda = [1.17 \mu\text{m}, 1.27 \mu\text{m}]$. The use of these bands reduces the bias by liquid water on light absorption by frozen water. This simple, yet powerful approach allows more robust retrievals of the optical snow grain size under snowmelt

conditions (Painter et al., 2013). Nevertheless, strong snowmelt with percolation of meltwater is assumed to introduce yet unknown bias to the snow grain size retrieval. More detailed studies of optical properties of melting snow would be required, such as Gallet et al. (2014) for example.

3.4 Snow albedo

5 ~~Albedo is a key parameter to the Earth's energy balance. The snow albedo feedback mechanism has a strong impact on climate on all temporal and spatial scales. In particular, snow albedo is a dominant driver of snowmelt, ecohydrological processes, as well as water supplies.~~

We derive the spectral snow albedo α_{snow}^{obs} from $HDRF_{snow}^{obs}$ by applying the anisotropy factor, which is given by the ratio between the modeled spectral albedo and the spectral $HDRF_{snow}^{mdl}$:

$$10 \alpha_{snow}^{obs}(r, \lambda) = \frac{HDRF_{snow}^{obs}(\theta_{\odot}, \theta_v, \varphi; r; \lambda) \alpha_{snow}^{mdl}(r, \lambda)}{HDRF_{snow}^{mdl}(\theta_{\odot}, \theta_v, \varphi; r; \lambda)} \quad (5)$$

The integration of Eq. (5) normalized by the topographically-modulated spectral total (direct + diffuse) irradiance at the surface level $E_{sfc}^{mdl}(\lambda, \theta_{\odot})$ derives the broadband (spectrally integrated) albedo as a function of the snow grain size r :

$$\alpha_{snow}^{obs}(r) = \frac{\int_{\lambda=0.36 \mu\text{m}}^{2.5 \mu\text{m}} E_{sfc}^{mdl}(\lambda, \theta_{\odot}) \alpha_{snow}^{obs}(r, \lambda) \Delta\lambda}{\int_{\lambda=0.36 \mu\text{m}}^{2.5 \mu\text{m}} E_{sfc}^{mdl}(\lambda, \theta_{\odot}) \Delta\lambda}. \quad (6)$$

$E_{sfc}^{mdl}(\lambda, \theta_{\odot})$ is provided ~~as an output from~~ with the direct and the diffuse component by the ATCOR-4 software (Painter et al., 15 2013; Richter and Schläpfer, 2014). Note that albedo values must range between 0 and 1, while HDRF can range up to 1.4 or even more.

3.5 Snow radiative forcing by light absorbing impurities

We calculate the radiative forcing by LAISI (RF) based on the difference between the observed spectral albedo and a modeled spectral clean snow albedo of the same grain radius (Painter et al., 2013). This reduction of spectral ~~albedo of snow by~~ 20 ~~impurities is wavelength-wise~~ snow albedo by LAISI is multiplied by the ~~total irradiance resulting in the~~ direct and diffuse instantaneous spectral solar irradiance entering the snow surface and integrated over the given spectrum, such that the the additional radiative flux into the snow pack is given by:

$$RF_{snow} = \int_{\lambda=0.36 \mu\text{m}}^{1.08 \mu\text{m}} E_{sfc}^{mdl}(\lambda, \theta_{\odot}) [\alpha_{snow}^{mdl}(r, \lambda) - \alpha_{snow}^{obs}(r, \lambda) c(r, \lambda_c)] \Delta\lambda, \quad (7)$$

where $c(r, \lambda_c) = \alpha_{snow}^{mdl}(r, \lambda_c) / \alpha_{snow}^{obs}(r, \lambda_c)$ denotes a scalar to adjust the modeled spectra to the measurements for a potential 25 bias by terrain modeling imperfections. c is derived at $\lambda_c = 1.08 \mu\text{m}$ where the influence of dust is relatively small (Warren and Wiscombe, 1980).

3.6 Estimates of the retrieval uncertainties

This study addresses mainly the qualitative nature of the snow property distribution in mountainous terrain. However, we have estimated the retrieval uncertainties based on the AVIRIS sensor performance (noise equivalent changes in radiance) and the retrieval method. The results were published by Painter et al. (2013), and we indicate, therefore, only the main points here. The uncertainties of snow grain size, albedo, and radiative forcing were estimated on the order of $\pm 25 \mu\text{m}$, ± 0.0001 (unitless), and $\pm 4 \text{ W m}^{-2}$, respectively. The modeled snow spectral reflectance is based on the assumption of spherical grains due to the use of the Mie theory (Mie, 1908). This assumption becomes more valid with grain growth associated with evolving metamorphism and rounding of the snow crystals. Nevertheless, strong snowmelt with percolation of meltwater is assumed to introduce yet unknown bias to the snow grain size retrieval. More detailed studies of optical properties of melting snow would be required, such as Gallet et al. (2014) for example. A further discussion on retrieval uncertainties is given in Sect. 4.5 based on the actual retrieval results.

4 Results

Figs. 4 to 6 show maps of snow grain size, albedo, and radiative forcing by LAISI in the Sierra Nevada (upper panel) and Rocky Mountains (lower panel) derived using algorithms described in Sect. 3 and Painter et al. (2013). The three dates represent an early, mid, and late observation during the melt period (see Fig. 3). These results are further analyzed in Sect. 4.1 regarding the temporal changes and in Sects. 4.2 to 4.4 regarding the spatial distribution and correlation with respect to elevation and aspect of the terrain.

4.1 Temporal changes of regional optical snow properties

In general, the snow line is significantly lower in the Sierra Nevada study area as compared to the Rocky Mountains because of the maritime snowpack. However, inter-annual variability also modulates the snow covered area. We calculate the snow covered area of the study area and normalize it by the basin area to serve as a proxy for accumulation and melt (Sect. 3.2). Figure 7 shows that the sequence of images in Kings/Kaweah captures the transition from an accumulating to melting snowpack, while it is mainly the melt season period in the Uncompahgre (refer also to Fig. 3). We can observe a difference between the two areas in the rate of snow cover change with respect to time, which is an indicator for the intensity of snowmelt. This is likely related to both the more frequent snowfall in the Kings/Kaweah in April and difference in solar irradiance between the March-April and May-June time periods.

The snowfall event between the first two airborne acquisitions observations in the Sierra Nevada also (Fig. 3) decreased the mean snow grain size from approximately 330 to $180 \mu\text{m}$, and then 330 to $180 \mu\text{m}$ (Fig. 7). The grain size varied little between the second and third acquisitions observation, after which it increased to $650 \mu\text{m}$ by the 4th and 5th acquisitions a month later. From the snow measurement sites we know observation to $650 \mu\text{m}$ within a month of time. We know from the SWE measurements at the surface sites that the transition to a melting snowpack likely occurred between these two acquisitions

(see after the second airborne observation (Fig. 3), while this tends to happen later at the higher elevations, such a large increase in grain size across the study area is not totally unexpected. See Sect. 5 for a discussion on the inverse relationship between snow grain size and elevation under intense snowmelt conditions.

Patterns in mean broadband albedo are similar to those exhibited-observed for grain size. The Sierra Nevada study site remained constant at around 0.7 due to late season snowfall until April and then decreased to 0.55 by the last two acquisitions in May, when the snowpack was melting. In the Rocky Mountain study area the mean snow albedo decreased from 0.75 in May to 0.5 in late June. In both areas the largest decreases were exhibited-observed in May, when both sites were likely undergoing the transition from the retention of cold content (below 0°C) to isothermal-transitioning to isothermal snowpack conditions (at 0°C) and melting.

The time-series of radiative forcing by LAISI are very similar for the two study areas, except that the values in the Rocky Mountains are roughly 20 W m^{-2} larger. This is consistent with the high dust concentrations in the Rocky Mountains (Skiles et al., 2012; Painter et al., 2012b) in combination with the increased solar irradiance later in the season.

4.2 Spatial distribution of snow grain size

Snow grain sizes at top of the snow pack are affected by snowfall, metamorphism, wind effects, and melt processes. We would expect to find smaller snow grains at higher elevation and north-oriented-north-facing slopes. With time, we also expect snow surface grain size to grow at varying rates, but decrease abruptly with the addition of snowfall. The analysis of our retrievals using Eq. (4) is consistent with this common theory. The two-dimensional histograms in Figs. 8 and 9 show the relation of grain size with elevation and with terrain aspect.

For both study areas we find for the early ablation period, that the snow grain size at high elevations is less than $200 \mu\text{m}$ and is $500\text{--}800 \mu\text{m}$ at low elevations. The snow grain size is inversely correlated with elevation in the May data of the Rocky Mountains. Snow grain size gradually increases over time at higher elevation as shown in the left panels of Figs. 8 and 9. Late in the ablation period the snow grain size is nearly constant with elevation, ranging from $500\text{--}700 \mu\text{m}$ and becomes positively, but less sensitively, correlated with elevation. Potential reasons for this remarkable change over time are discussed in Sect. 5. The snow grain size distribution with respect to the terrain orientation (aspect) is shown in the right panels of Figs. 8 and 9. As expected, we retrieve small snow grain sizes, on the order of about $100\text{--}100 \mu\text{m}$ on north facing slopes, versus $400\text{--}400 \mu\text{m}$ or more on south-east slopes. On 5 March 2009, just after a snow event, the snow grain sizes are significantly smaller with a small and have relatively low spatial variability, especially at higher elevations. More pixels at lower elevations were covered with snow (see Fig. 8).

4.3 Spatial distribution of snow albedo

The reflectivity of snow determines how much solar irradiance is absorbed, which provides the most energy for reduction of cold content and melting. Imaging spectroscopy data allow us to derive the HDRF (Eq. 1), and from that metric the spectrally integrated albedo with a snow reflectance model (Eq. 6). The broadband albedo is directly relevant to the energy balance in a snowpack and, therefore, a main product of our retrievals (see Sect. 3).

Snow albedo is correlated with elevation and terrain aspect early in the ablation period at both study areas (see Figs. 10 through 13). Our retrievals in the early ablation period show albedo values of 0.6 to 0.8 at higher elevations, and 0.5 to 0.6 at lower elevations for both study areas. A rather large spatial variance is observed in ~~the~~ February, March and April ~~data~~ in the Sierra Nevada as shown in Fig. (10) with albedo varying from 0.5 to almost 0.9 within less than a kilometer. In each case the higher albedo values are found on north and steep west facing slopes. Later in the ablation period, albedo values decreased to approximately 0.5 and 0.4 at high and low elevations, respectively. In general the albedo increase with elevation is more distinct at the Sierra Nevada study area than in the Rocky Mountain study area. A strong dependence of snow albedo with terrain slope is found in February and March in the Sierra Nevada. North facing slopes show values ranging between 0.8 and 0.9, whereas south facing slopes are clearly darker with approximately 0.6 albedo values (Figs. 10 and 12). We found similar, although less distinct, dependencies in the Rocky Mountains (Figs. 11 and 13). This is likely because northern slopes experience larger relative changes in irradiance during spring due to a decrease in solar zenith angle and the related reduction of terrain shadows. The Rocky Mountain study area observations were started in May, so the terrain effects are less prominent than those of the Sierra Nevada study area, which were started in February. During the late ablation period the differences in snow albedo between north and south facing slopes was less than 0.1.

In both time-series the spatial variance in the retrieved albedo corresponds with the spatial variance in retrieved snow grain sizes (see Fig. 7). For example, the retrievals on 5 March 2009, just after the snowfall event, show ~~a increased variances an~~ increased variance in both albedo and grain size (see Fig. 12).

4.4 Spatial distribution of radiative forcing

We find the radiative forcing by LAISI increasing during ablation from almost zero to spatial mean values of 170 W m^{-2} in the Sierra Nevada and 190 W m^{-2} in the Rocky Mountains (Figs. 7, 14, and 15). The standard deviations are in the order of 60 W m^{-2} in both study areas across the full period. The Colorado data were acquired later in spring than the California data, and thus with more solar irradiance. A direct quantitative comparison of radiative forcing between the two datasets is therefore difficult. The higher elevations in Colorado contribute to a later onset of snowmelt as compared to the Sierra Nevada, which leads to a later exposure of LAISI at the surface of the snowpack. We should bear in mind that each year is different in terms of dust deposition and exposure at the surface (Painter et al., 2012b). Nevertheless a qualitative comparison with changes in snow water equivalent (Fig. 3), as an indicator for snow accumulation and snowmelt, shows a relationship of longer snowmelt periods with an increase in radiative forcing. This ~~is likely due to higher impurity content in the Rocky Mountains, and~~ could be dominated by the SWE magnitude with a longer time period over which impurities can be deposited and then accumulated at the surface. It could also be due to higher impurity content in the Rocky Mountains or a combination of both. In 2011 only three of the observed dust events occurred between the first and last flights in the Rocky Mountains, but all of the dust deposited over the full season would have surfaced as snow started to melt likely contributing to the higher radiative forcings in this area.

In California, we found almost no dependence of radiative forcing on elevation (Fig. 14). In contrast, the radiative forcing retrieved in Colorado is clearly correlated with respect to elevation with a distinct trend of larger radiative forcing at lower

elevations (Fig. 15). Column 2 of Figs. 14 and 15 shows the radiative forcing with respect to the terrain aspect. In the northern hemisphere, south facing slopes experience stronger irradiance and decreased snow albedo values (Sect. 4.3). The combination of both of these factors, in addition to LAISI deposition, led to increased radiative forcing. For example, in the Sierra Nevada, the radiative forcing is close to zero until May at northern slopes and up to about ~~150 W m⁻²~~ 150 W m⁻² at south-south-eastern aspects. In May, we retrieve up to ~~150 W m⁻²~~ 150 W m⁻² at northern slopes and about ~~200 W m⁻²~~ 200 W m⁻² at southern oriented terrain slopes (Fig. 14). The analysis of the Rocky Mountain study area shows a similar trend over time, but with radiative forcing values ~~50 W m⁻² to 100 W m⁻²~~ 50 W m⁻² to 100 W m⁻² larger than in the Sierra Nevada (Fig. 15). We also find that the dependence of terrain aspect angle with radiative forcing decreases until the summer solstice due to the decreasing solar zenith angle and the corresponding irradiance increase on steep slopes in mountainous terrain. Our results show radiative forcing differences between north and south facing slopes being smoothed out over time. An exception is found in late June in Colorado with significantly larger radiative forcing on south-east slopes of up to ~~300 W m⁻²~~ 300 W m⁻². This is presumably due to the earlier melt out of south to south-west slopes and may also be due to dust transport effects.

4.5 Uncertainty and error analysis

~~An indirect estimation of the data~~ Painter et al. (2013) reported baseline retrieval uncertainties based on the AVIRIS sensor performance (noise-equivalent changes in radiance or NE Δ L) of ± 0.001 , $\pm 3.6 \mu\text{m}$ (at the $1.03 \mu\text{m}$ ice absorption feature), and $\pm 0.2 \text{ W m}^{-2}$ for albedo, grain size, and radiative forcing by LAISI, respectively. When compared to two in situ measurements, Painter et al. (2013) found an albedo retrieval error of less than 0.005 and a radiative forcing error of about $2 \pm 5 \text{ W m}^{-2}$. The grain size retrieval error for the smaller grains is assumed to be on the order of $\pm 25 \mu\text{m}$ (Nolin and Dozier, 2000). As mentioned in Sect. 3.3, further investigations are needed to quantify the grain size retrieval accuracy under melting snow conditions. While inherent snow albedo is controlled by grain size and impurity content over the course of a day, the solar zenith angle, cloud cover, and topography also act to influence albedo and net solar radiation (Warren, 1982). For our acquisitions, we account for local illumination and view geometries in the albedo retrievals (Eqs. 2 and 5).

Additional error sources are related to terrain shadows and the digital elevation model (Sect. 2.1). Up to 10% of the snow pixels in the February data are in shadow due to the large solar zenith angle. Snow properties can be retrieved in shadows using the diffuse irradiance. However, we suspect that large uncertainties are introduced due to adjacency effects, which are difficult to model in snow covered mountains. We therefore remove retrievals in shadow areas from our analysis, except for the snow cover calculation. Pixels very close to a ridge can be assigned an incorrect aspect value, which causes retrieval outliers. We found only very few snow pixels affected by this artifact and they do not show up in the histogram plots (Figs. 8, 9, and 12-15) due to a threshold of 15 occurrences. Changes in slope and aspect of the surface due to snow accumulation are not taken into account in this study and further analysis would be required to quantify associated errors.

To estimate the data quality and retrieval robustness~~can be performed by~~, we performed an analysis of the variance of the retrieved quantities on timescales shorter than the natural variability. For example, the last two Sierra Nevada datasets are a single day apart and the snow products were retrieved with almost identical values. ~~The (relative) differences between 8 May and 9 May are -2.8 km^2 (-1%) snow cover~~, Between 7 May and 8 May the snow cover area has decreased by 2.8 km^2 or about

1% of the mean. With a sample size of more than 280000 snow pixels, the mean, percent difference (in brackets), and \pm one standard deviation of the differences in albedo, grain size, and radiative forcing are roughly $-0.01(-2\%)$ albedo $0.5\% \pm 0.04$, $+35 \mu\text{m}(34(1.3\%) \pm 112 \mu\text{m}, +5\%)$ grain size, and $+3 \text{ W m}^{-2}(+2\%)$ radiative forcing (see $5(0.8\%) \pm 26 \text{ W m}^{-2}$ (see also Fig. 7). These are all plausible values, which can be at least partly attributed to physical processes as opposed to substantial errors.
5, respectively. These values are in the same order of magnitude as the expected retrieval accuracy (Painter et al., 2013). Nevertheless, the quantities and their signs show plausible values for changes in snow properties from one day to another at the end of the ablation period.

An additional source of errors is the insufficiently spatially-resolved digital elevation model. The elevation model used in this study was interpolated (cubic convolution) from 30 m (Sect. 2.1) to the actual pixel size of each AVIRIS flight line, which is on the order of 2 to 15 m (Tab. 2). Terrain effects are also a source of errors, especially if shadow areas in steep terrain are not correctly accounted for. As a mitigation, we have masked retrievals in shadow areas, except for the snow cover calculations. Up to 10% of the snow pixels are affected by terrain shadows in the February data due to large solar zenith angles. The shadows increase the variance, or noise, in the retrieval products.

5 Inverse relationship of grain size with elevation of melting snow

15 As grain sizes in a dry snowpack are primarily driven by metamorphism, ~~itself~~ which is driven by temperature and vapor pressure gradients, we expect increased snow grain sizes at lower elevations because of warmer temperature and ~~higher positive~~ a greater positive snowpack energy balance. This is in agreement with our observations shown in Figs. 8 and 9 of the initial ablation ~~season~~ period, while they remain mostly unchanged at lower elevations. In the Sierra Nevada this is apparent in the 20 May acquisitions relative to the April acquisition. In the Rocky Mountains this is apparent in the June acquisitions. Later in the ablation ~~season~~ period, with increased solar irradiance, the snow grain size distribution becomes independent of the terrain aspect.

We suggest that there are two processes that account for these observations. First, ~~that~~ changes in grain size are slowest when the snowpack is both cold and when it is fully isothermal, and most rapid during the transition between these two phases (Taillandier et al., 2007). When the grain growth is slow at lower elevations, but rapid at higher elevations, this indicates that lower elevations have become isothermal while the upper elevations are still undergoing that transition. Grain growth can be rapid in cold snowpacks, but this tends to occur near the ground where the temperature gradient between the ground and snow is greatest, and not at the surface. When liquid water is ~~present~~ present, snow grains tend to appear visually larger because they form clusters but optically the absorbing path length seems to change very little. This same slowing of grain growth rates 30 after the isothermal transition was observed ~~by Skiles (2014)~~ in daily vertical profiles of optical snow grain size over the 2013 ~~ablations season in~~ ablation period in the Senator Beck Basin (Skiles, 2014).

Second, when there is an actual inversion of grain sizes with elevation, we suggest this is accounted for by rapid melt induced by high impurity content at the surface. ~~This~~ Although the change in grain size is on the order of the uncertainty in grain size

retrieval, it is not the absolute values that are important but rather the trend. A decrease in surface grain size in the presence of high impurity content

was also observed in the daily field observations in 2013 by Skiles (2014), when the dust layers coalesced at the surface and skies were clear both grain sizes and density in the surface layers decreased and surface roughness increased. ~~These observations~~ Skiles (2014), Painter et al. (2013) and the results in this paper suggest that the intensification of snowmelt by dust in the visible wavelengths results in destructive metamorphism near the snow-atmosphere interface and snowmelt infiltration with refreezing and snow grain coarsening at depths of ca. 2–10 cm. The observed snow grains in the near-surface layer can therefore be smaller under intense snowmelt. The results could also suggest that sublimation could form frost flower-like crystals on the surface of a refreezing surface layer resulting in an increase of SSA and a decrease in snow grain size (Domine et al., 2005).

10 In addition, our analyses confirm the inverse correlation between the snow albedo and grain size distribution (Flanner and Zender, 2006). Smaller snow grains have smaller absorbing path lengths and smaller single-scattering asymmetry parameters (more side-scattering), which combined lead to higher snow albedo. We find in our results a similar inverse correlation between snow albedo and RF. The quantitative relationships between radiative forcing and the spatial and temporal parameters can vary with respect to snow albedo due to the differences in the local instantaneous solar irradiance.

15 6 Conclusions

Snow cover across the worlds mountainous regions is important for both regional climate and hydrology. Snow albedo, itself controlled by impurity content and grain size, is particularly relevant for understanding melt initiation and melt rates. Ongoing consistent measurements of snow albedo only occur at six snow energy balance sites across the western US, with even sparser or nonexistent measurements globally (Painter et al., 2012b). The analysis of the snow remote sensing products presented here, derived from a series of imaging spectroscopy data, provides new insights into the spatial distribution of snow albedo and snow optical properties at five time steps across the accumulation/ablation transition in the Sierra Nevada and across the ablation ~~season~~ period in the Rocky Mountains. The focus of most of the publications on snow property retrievals from imaging spectrometer data (see Sect. 3) has been on algorithm development and technology demonstration. Here we take the next step, utilizing the proven data and algorithms to assess spatial and temporal patterns. While some of our results are intuitive, such as smaller grain sizes on north facing slopes and the inverse relationship between grain size and albedo, other were counterintuitive, including faster grain growth rates at higher elevations and higher grain sizes at high elevations relative to lower elevations late in the ablation ~~season. This is the first time we have been to analyze patterns like these at this spatial and spectral scale.~~ period. this

The retrieval of impurity radiative forcing is especially relevant as efforts are now in place to reduce short-lived climate pollutants, such as black carbon, brown carbon, methane, tropospheric ozone and some hydrofluorocarbons by the Climate and Clean Air Coalition managed by the United Nations Environmental Programme (Shindell et al., 2011). It will become critical to monitor these short-lived climate pollutants with respect to their spatial distribution on the local to global scale, as well as their change in time. Additional studies of the spatial and temporal distribution of impurity content in snow and ice of large

mountain ranges, boreal and arctic regions are needed to enable ~~us to improve our~~ improved understanding of snow in the framework of complex climate-terrain feedbacks. The application of our methods and algorithms to airborne and upcoming spaceborne imaging spectrometer data, such as the Hyperspectral Infrared Imager (HyspIRI), are potential tools to address this important question.

- 5 ~~In addition, further application of the data and algorithms described here and in Painter et al. (2013) could provide valuable insights for water resources management to increase hydropower generation efficiency and to help better secure drinking water availability. As an example, NASA's Airborne Snow Observatory (Painter et al., 2015) applies these retrieval methods operationally to quantify snow optical properties in the full Tuolumne River basin, Sierra Nevada, California, on a weekly basis throughout the ablation periods of years 2013 to 2015. In this case, additional LiDAR data are being used to also quantify snow~~
- 10 ~~hydrology parameters, such as snow depth and SWE.~~

Author contributions. F.C. Seidel wrote and applied the retrieval codes to derive the snow products, which are based on original algorithms by T.H. Painter. K. Rittger prepared the AVIRIS and snow pillow data. S. M. Skiles contributed content related to snow hydrology. N.P. Molotch was the investigator for the Southern Sierra Snow Survey flights. F.C. Seidel prepared the manuscript with contributions from all co-authors.

- 15 *Acknowledgements.* This research was performed at the Jet Propulsion Laboratory, California Institute of Technology, under a contract with the National Aeronautics and Space Administration. Thanks to ~~Dr. Noah Molotch as the investigator for the Southern Sierra Snow Survey flights with the ER-2, to the~~ the AVIRIS and ER-2 teams, ~~and as well as to~~ as well as to Dr. Peter Kirchner for useful discussions. Copyright 2016 California Institute of Technology. All Rights Reserved 2016.

References

- Bales, R. C., Molotch, N. P., Painter, T. H., Dettinger, M. D., Rice, R., and Dozier, J.: Mountain hydrology of the western United States, *Water Resources Research*, 42, n/a–n/a, doi:10.1029/2005WR004387, <http://dx.doi.org/10.1029/2005WR004387>, 2006.
- Domine, F., Taillandier, A. S., Simpson, W. R., and Severin, K.: Specific surface area, density and microstructure of frost flowers, *Geophysical Research Letters*, 32, n/a–n/a, doi:10.1029/2005GL023245, <http://dx.doi.org/10.1029/2005GL023245>, 2005.
- 5 Dozier, J.: Spectral signature of alpine snow cover from the landsat thematic mapper, *Remote Sensing of Environment*, 28, 9 – 22, doi:[http://dx.doi.org/10.1016/0034-4257\(89\)90101-6](http://dx.doi.org/10.1016/0034-4257(89)90101-6), 1989.
- Dozier, J. and Marks, D.: Snow mapping and classification from Landsat Thematic Mapper data, *Annals of Glaciology*, 9, 97–103, 1987.
- Dozier, J., Green, R. O., Nolin, A. W., and Painter, T. H.: Interpretation of snow properties from imaging spectrometry, *Remote Sensing of Environment*, 113, Supplement 1, S25–S37, doi:<http://dx.doi.org/10.1016/j.rse.2007.07.029>, <http://www.sciencedirect.com/science/article/pii/S0034425709000777>, 2009.
- 10 Flanner, M. G. and Zender, C. S.: Linking snowpack microphysics and albedo evolution, *Journal of Geophysical Research: Atmospheres*, 111, n/a–n/a, doi:10.1029/2005JD006834, <http://dx.doi.org/10.1029/2005JD006834>, 2006.
- Flanner, M. G., Zender, C. S., Hess, P. G., Mahowald, N. M., Painter, T. H., Ramanathan, V., and Rasch, P. J.: Springtime warming and reduced snow cover from carbonaceous particles, *Atmospheric Chemistry and Physics*, 9, 2481–2497, doi:10.5194/acp-9-2481-2009, 2009.
- 15 Gallet, J. C., Domine, F., Zender, C. S., and Picard, G.: Measurement of the specific surface area of snow using infrared reflectance in an integrating sphere at 1310 and 1550 nm, *The Cryosphere*, 3, 167–182, doi:10.5194/tc-3-167-2009, <http://www.the-cryosphere.net/3/167/2009/>, 2009.
- 20 Gallet, J. C., Domine, F., and Dumont, M.: Measuring the specific surface area of wet snow using 1310 nm reflectance, *The Cryosphere*, 8, 1139–1148, doi:10.5194/tc-8-1139-2014, <http://www.the-cryosphere.net/8/1139/2014/>, 2014.
- Garen, D. C. and Marks, D.: Spatially distributed energy balance snowmelt modelling in a mountainous river basin: estimation of meteorological inputs and verification of model results, *Journal of Hydrology*, 315, 126 – 153, doi:<http://dx.doi.org/10.1016/j.jhydrol.2005.03.026>, 2005.
- 25 Green, R. O., Painter, T. H., Roberts, D. A., and Dozier, J.: Measuring the expressed abundance of the three phases of water with an imaging spectrometer over melting snow, *Water Resources Research*, 42, W10402, doi:10.1029/2005WR004509, <http://dx.doi.org/10.1029/2005WR004509>, 2006.
- Hall, D. K., Riggs, G. A., Salomonson, V. V., DiGirolamo, N. E., and Bayr, K. J.: MODIS snow-cover products, *Remote Sensing of Environment*, 83, 181–194, doi:[http://dx.doi.org/10.1016/S0034-4257\(02\)00095-0](http://dx.doi.org/10.1016/S0034-4257(02)00095-0), <http://www.sciencedirect.com/science/article/pii/S0034425702000950>, 2002.
- 30 Leppänen, L., Kontu, A., Vehviläinen, J., Lemmetyinen, J., and Pulliainen, J.: Comparison of traditional and optical grain-size field measurements with SNOWPACK simulations in a taiga snowpack, *Journal of Glaciology*, 61, 151–162, doi:10.3189/2015JogG14J026, 2015.
- Link, T. E. and Marks, D.: Point simulation of seasonal snow cover dynamics beneath boreal forest canopies, *Journal of Geophysical Research: Atmospheres*, 104, 27 841–27 857, doi:10.1029/1998JD200121, 1999.
- 35 Marks, D. and Dozier, J.: Climate and energy exchange at the snow surface in the Alpine Region of the Sierra Nevada: 2. Snow cover energy balance, *Water Resources Research*, 28, 3043–3054, doi:10.1029/92WR01483, 1992.

- Mie, G.: Beiträge zur Optik trüber Medien, speziell kolloidaler Metallösungen, *Annalen der Physik*, 330, 377–445, doi:10.1002/andp.19083300302, 1908.
- Molotch, N. P., Painter, T. H., Bales, R. C., and Dozier, J.: Incorporating remotely-sensed snow albedo into a spatially-distributed snowmelt model, *Geophysical Research Letters*, 31, n/a–n/a, doi:10.1029/2003GL019063, <http://dx.doi.org/10.1029/2003GL019063>, 2004.
- 5 Nolin, A. W. and Dozier, J.: A Hyperspectral Method for Remotely Sensing the Grain Size of Snow, *Remote Sensing of Environment*, 74, 207 – 216, doi:[http://dx.doi.org/10.1016/S0034-4257\(00\)00111-5](http://dx.doi.org/10.1016/S0034-4257(00)00111-5), 2000.
- Oerlemans, J.: Analysis of a 3 year meteorological record from the ablation zone of Morteratschgletscher, Switzerland: energy and mass balance, *Journal of Glaciology*, 46, 571–579, doi:10.3189/172756500781832657, 2000.
- Painter, T. H. and Dozier, J.: The effect of anisotropic reflectance on imaging spectroscopy of snow properties, *Remote Sensing of Environment*, 89, 409–422, doi:<http://dx.doi.org/10.1016/j.rse.2003.09.007>, <http://www.sciencedirect.com/science/article/pii/S0034425703002578>, 2004.
- 10 Painter, T. H., Duval, B., Thomas, W. H., Mendez, M., Heintzelman, S., and Dozier, J.: Detection and Quantification of Snow Algae with an Airborne Imaging Spectrometer, *Applied and Environmental Microbiology*, 67, 5267–5272, doi:10.1128/AEM.67.11.5267-5272.2001, <http://aem.asm.org/content/67/11/5267.abstract>, 2001.
- 15 Painter, T. H., Dozier, J., Roberts, D. A., Davis, R. E., and Green, R. O.: Retrieval of subpixel snow-covered area and grain size from imaging spectrometer data, *Remote Sensing of Environment*, 85, 64 – 77, doi:[http://dx.doi.org/10.1016/S0034-4257\(02\)00187-6](http://dx.doi.org/10.1016/S0034-4257(02)00187-6), 2003.
- Painter, T. H., Barrett, A. P., Landry, C. C., Neff, J. C., Cassidy, M. P., Lawrence, C. R., McBride, K. E., and Farmer, G. L.: Impact of disturbed desert soils on duration of mountain snow cover, *Geophysical Research Letters*, 34, L12 502, doi:10.1029/2007GL030284, 2007a.
- Painter, T. H., Molotch, N. P., Cassidy, M. P., Flanner, M. G., and Steffen, K.: Contact spectroscopy for the determination of stratigraphy of snow grain size, *Journal of Glaciology*, 53, 121–127, 2007b.
- 20 Painter, T. H., Deems, J. S., Belnap, J., Hamlet, A. F., Landry, C. C., and Udall, B.: Response of Colorado River runoff to dust radiative forcing in snow, *Proceedings of the National Academy of Sciences*, 107, 17 125–17 130, doi:10.1073/pnas.0913139107, 2010.
- Painter, T. H., Bryant, A. C., and Skiles, S. M.: Radiative forcing by light absorbing impurities in snow from MODIS surface reflectance data, *Geophysical Research Letters*, 39, L17 502, doi:10.1029/2012GL052457, 2012a.
- 25 Painter, T. H., Skiles, S. M., Deems, J. S., Bryant, A. C., and Landry, C. C.: Dust radiative forcing in snow of the Upper Colorado River Basin: 1. A 6 year record of energy balance, radiation, and dust concentrations, *Water Resources Research*, 48, W07 521, doi:10.1029/2012WR011985, 2012b.
- Painter, T. H., Seidel, F. C., Bryant, A. C., McKenzie Skiles, S., and Rittger, K.: Imaging spectroscopy of albedo and radiative forcing by light-absorbing impurities in mountain snow, *Journal of Geophysical Research: Atmospheres*, 118, 9511–9523, doi:10.1002/jgrd.50520, 30 2013.
- Painter, T. H., Berisford, D., Boardman, J. W., Bormann, K. J., Deems, J. S., Gehrke, F., Hedrick, A., Joyce, M., Laidlaw, R. K., Marks, D., Mattmann, C., McGurk, B., Ramirez, P., Richardson, M., Seidel, F. C., Skiles, S. M., and Winstral, A.: The Airborne Snow Observatory: scanning lidar and imaging spectrometer fusion for mapping snow water equivalent and snow albedo, *Remote Sensing of Environment*, (Submitted), 2015.
- 35 Qian, Y., Gustafson, W. I., Leung, L. R., and Ghan, S. J.: Effects of soot-induced snow albedo change on snowpack and hydrological cycle in western United States based on Weather Research and Forecasting chemistry and regional climate simulations, *Journal of Geophysical Research: Atmospheres*, 114, D03 108, doi:10.1029/2008JD011039, 2009.

- Qian, Y., Yasunari, T., Doherty, S., Flanner, M., Lau, W. M., Ming, J., Wang, H., Wang, M., Warren, S., and Zhang, R.: Light-absorbing particles in snow and ice: Measurement and modeling of climatic and hydrological impact, *32*, 64–91, doi:10.1007/s00376-014-0010-0, 2015.
- Ramanathan, V., Ramana, M. V., Roberts, G., Kim, D., Corrigan, C., Chung, C., and Winker, D.: Warming trends in Asia amplified by brown cloud solar absorption, *Nature*, *448*, 575–578, 2007.
- Richter, R. and Schläpfer, D.: Atmospheric / Topographic Correction for Airborne Imagery. ATCOR-4 Userguide 6.3.2, DLR, Wessling, Germany, 2014.
- Schaepman-Strub, G., Schaepman, M., Painter, T., Dangel, S., and Martonchik, J.: Reflectance quantities in optical remote sensing—definitions and case studies, *Remote Sensing of Environment*, *103*, 27 – 42, doi:10.1016/j.rse.2006.03.002, 2006.
- 10 Shindell, D., Kuylenstierna, J. C. I., Hicks, K., Raes, F., Ramanathan, V., Rosenthal, E., Terry, S., and Williams, M.: Integrated Assessment of Black Carbon and Tropospheric Ozone: Summary for Decision Makers, UNEP/WMO, Nairobi, Kenya, 2011.
- Skiles, S. M.: Dust and Black Carbon Radiative Forcing Controls on Snowmelt in the Colorado River Basin, Ph.D. thesis, University of California-Los Angeles, Los Angeles, 2014.
- Skiles, S. M., Painter, T. H., Deems, J. S., Bryant, A. C., and Landry, C. C.: Dust radiative forcing in snow of the Upper Colorado River Basin: 2. Interannual variability in radiative forcing and snowmelt rates, *Water Resources Research*, *48*, W07 522, doi:10.1029/2012WR011986, 15 2012.
- Skiles, S. M., Painter, T. H., Belnap, J., Holland, L., Reynolds, R., Goldstein, H. L., and Lin, J. C.: Regional variability in dust on snow processes and impacts in the upper Colorado River Basin, *Hydrologic Processes*, In Review, 2015.
- Stamnes, K., Tsay, S.-C., Wiscombe, W., and Jayaweera, K.: Numerically stable algorithm for discrete-ordinate-method radiative transfer in multiple scattering and emitting layered media, *Applied Optics*, *27*, 2502, doi:10.1364/AO.27.002502, <http://ao.osa.org/abstract.cfm?URI=ao-27-12-2502>, 1988.
- 20 Sterle, K. M., McConnell, J. R., Dozier, J., Edwards, R., and Flanner, M. G.: Retention and radiative forcing of black carbon in eastern Sierra Nevada snow, *The Cryosphere*, *7*, 365–374, doi:10.5194/tc-7-365-2013, <http://www.the-cryosphere.net/7/365/2013/>, 2013.
- Sturm, M., Holmgren, J., and Liston, G. E.: A Seasonal Snow Cover Classification System for Local to Global Applications, *Journal of Climate*, *8*, 1261–1283, doi:10.1175/1520-0442(1995)008<1261:ASSCCS>2.0.CO;2, [http://dx.doi.org/10.1175/1520-0442\(1995\)008<1261:ASSCCS>2.0.CO;2](http://dx.doi.org/10.1175/1520-0442(1995)008<1261:ASSCCS>2.0.CO;2), 1995.
- 25 Taillandier, A.-S., Domine, F., Simpson, W. R., Sturm, M., and Douglas, T. A.: Rate of decrease of the specific surface area of dry snow: Isothermal and temperature gradient conditions, *Journal of Geophysical Research: Earth Surface*, *112*, n/a–n/a, doi:10.1029/2006JF000514, <http://dx.doi.org/10.1029/2006JF000514>, 2007.
- 30 Warren, S. G.: Optical properties of snow, *Reviews of Geophysics*, *20*, 67–89, doi:10.1029/RG020i001p00067, <http://dx.doi.org/10.1029/RG020i001p00067>, 1982.
- Warren, S. G. and Wiscombe, W. J.: A Model for the Spectral Albedo of Snow. II: Snow Containing Atmospheric Aerosols, *Journal of the Atmospheric Sciences*, *37*, 2734–2745, doi:10.1175/1520-0469(1980)037<2734:AMFTSA>2.0.CO;2, 1980.

Table 1. Data parameters of the study areas derived as a mosaic from the subsets of flight lines (see Table 2 and Fig. 1).

Sierra Nevada, CA. 2009	
Dates	27 Feb., 05 Mar., 04 Apr., 07 May, 08 May
Pixel Size [m]	14.5
Image Area [km ² ,pixels]	252.03067, 1.2 · 10⁶ <u>252.03067, 1.2 · 10⁶</u>
Elevation Min./Mean/Max. [m]	1140 / 2575 / 3533
Rocky Mountains, CO. 2011	
Dates	13 May, 16 May, 09 Jun., 15 Jun., 23 Jun
Pixel Size [m]	13.8
Image Area [km ² ,pixels]	54.721982, 2.9 · 10⁵ <u>54.721982, 2.9 · 10⁵</u>
Elevation Min./Mean/Max. [m]	2950 / 3605 / 4111

Table 2. Summary of the individual AVIRIS scenes used in this paper. The scene number corresponds to the AVIRIS ‘run ID’. The aircraft altitude, heading, and the terrain elevation are averages per scene. The solar geometry is valid at the center of a scene. Water vapor is retrieved using ATCOR-4 (see Sect. 3).

AVIRIS		Aircraft		Mean	Pixel	Solar		Water
Flight Date	Scene Nr.	Altitude [km]	Heading [deg.]	Elevation [km]	Size [m]	Zenith [deg.]	Azimuth [deg.]	Vapor [cm]
Sierra Nevada, CA. 2009								
27 Feb	6	19.799	354	2.547	14.1	48.3	205.7	0.32
	8	19.836	185	2.925	13.9	56.1	205.4	0.23
05 Mar	5	19.806	181	2.056	14.4	45.7	155.3	0.22
	6	19.765	000	2.554	14.0	44.7	158.7	0.13
	7	19.773	181	2.879	13.7	44.1	162.7	0.09
04 Apr	5	19.799	182	2.082	14.4	41.0	131.6	0.16
	6	19.674	359	2.552	13.9	39.5	134.4	0.10
	7	19.902	181	2.911	13.8	38.5	137.3	0.07
	8	19.796	000	1.865	14.5	37.4	139.7	0.24
07 May	6	14.262	348	3.020	9.0	23.4	144.0	0.30
	7	14.274	193	2.650	9.3	22.4	148.6	0.43
	8	14.273	349	2.277	9.3	21.5	154.4	0.62
08 May	5	14.141	343	3.178	8.9	27.6	129.0	0.36
	6	14.154	194	2.642	9.2	26.4	132.2	0.55
	7	14.154	345	2.383	9.2	25.0	136.4	0.73
	8	14.144	195	2.035	9.6	23.9	140.7	0.89
	9	14.157	346	2.715	9.2	22.6	146.1	0.58
Rocky Mountains, CO. 2011								
13 May	5	6.496	352	3.560	2.1	19.6	173.0	0.25
	6	6.536	354	3.526	2.1	19.5	182.9	0.25
	7	6.533	354	3.683	2.1	19.9	192.6	0.21
16 May	7	19.866	180	3.237	13.5	20.5	153.5	0.22
09 Jun	12	20.170	179	3.260	13.7	15.0	179.1	0.33
15 Jun	12	20.216	180	3.196	13.8	20.8	129.7	0.51
23 Jun	5	20.139	001	3.271	13.7	38.3	102.0	0.54

FCSeidel-f01.pdf

Figure 1. Geographic extend of the AVIRIS image data. The study area is shown hatched. It is based on a mosaic of subsets, such that a common area exists for all flight dates. The elevation model is hill shaded in the background with an illumination corresponding to the mean solar position for all dates.

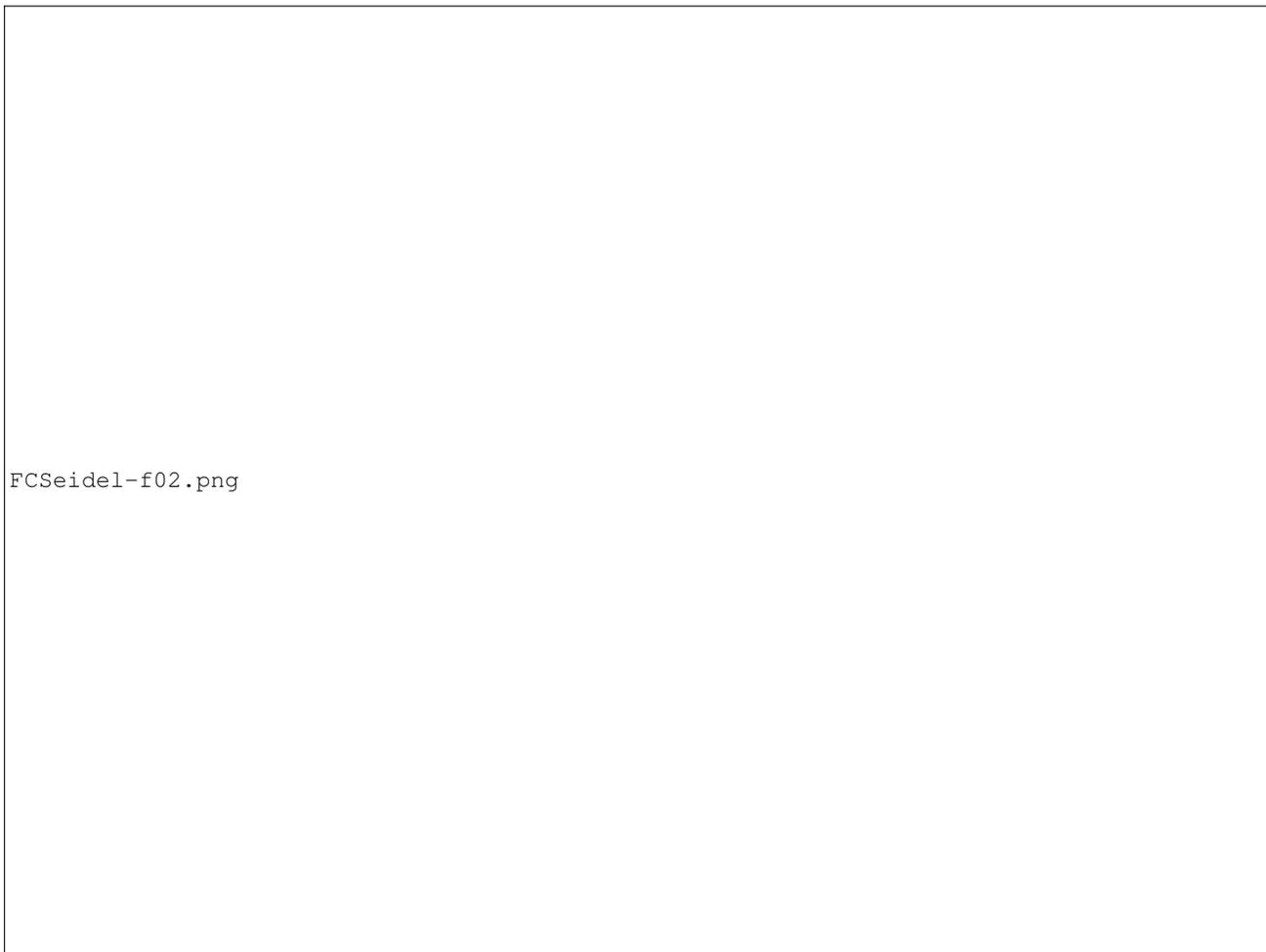


Figure 2. Histograms of the terrain aspect (top) and elevation (bottom) for the two study sites, Kings/Kaweah Basin Sierra Nevada, CA. (left) and Uncompahgre Basin Rocky Mountains, CO. (right). The values are normalized by the size of the study area given in Table 1. The peak occurrences of terrain aspect give an indication to the main drainage direction of a river basin.

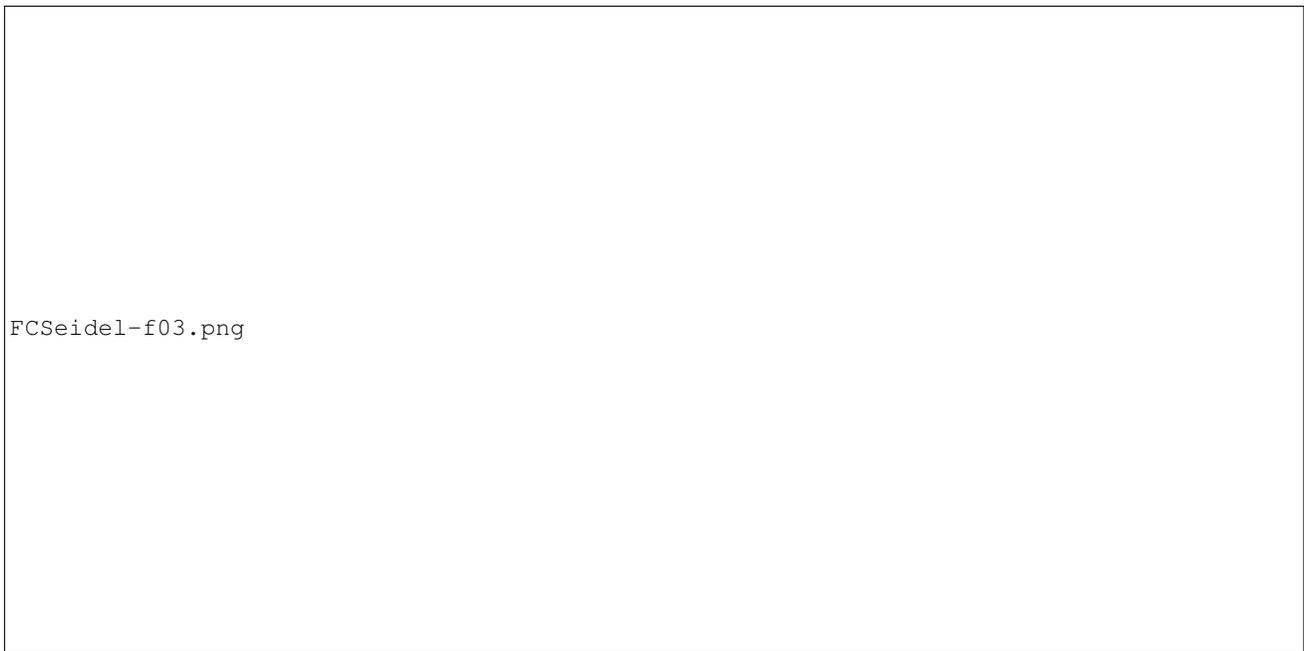


Figure 3. Snow accumulation (blue) and snowmelt (red) indicated with the differential Snow Water Equivalent (Δ SWE) with respect to time. The AVIRIS flight dates are marked with black vertical lines and a symbol indicating the ER-2 or Twin-Otter airborne platform. The upper plot shows snow sensor pillow data from two stations representing a higher and a lower location in the Sierra Nevada, CA, study area in 2009. The lower plot shows the same information, but from stations close to the Rocky Mountains, CO, study area in 2011.



Figure 4. Maps of snow grain size retrieved using Eq. (4) for three dates during the melt period in the Sierra Nevada (upper panel), and the Rocky Mountains (lower panel). The upper and lower map represent 252 km² and 55 km², respectively (Table. 1).



Figure 5. Same as Fig. 4 but for snow albedo.

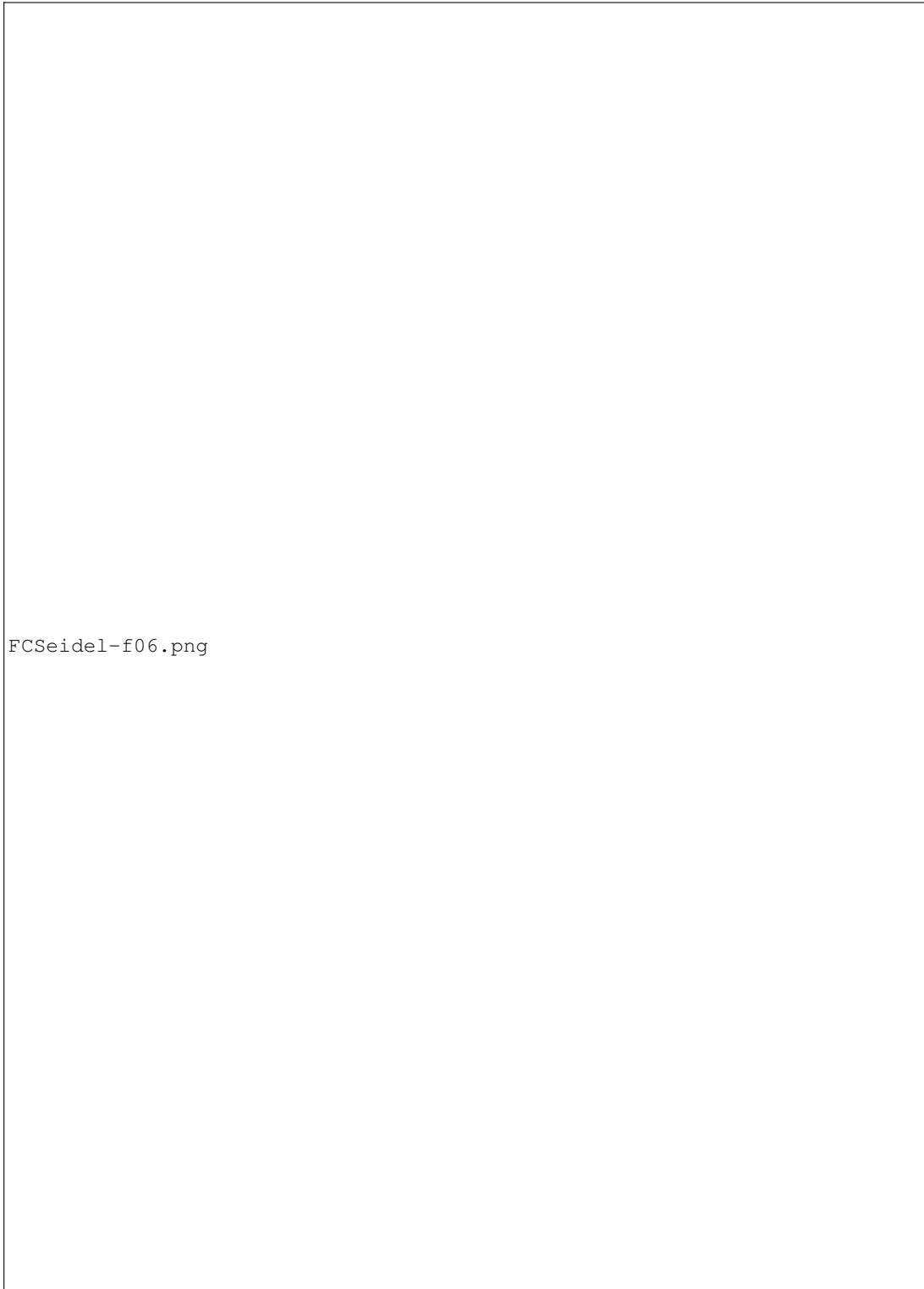


Figure 6. Same as Fig. 4 but for snow radiative forcing.



Figure 7. Time-series of snow cover, albedo, grain size and [impurity](#) radiative forcing in the Sierra Nevada, CA., USA in 2009 (upper panel), and in the Rocky Mountains, Co., USA in 2011 (lower panel). The snow cover is normalized by the size of the study area and the other values represent the average value per date surrounded by the corresponding standard deviation.

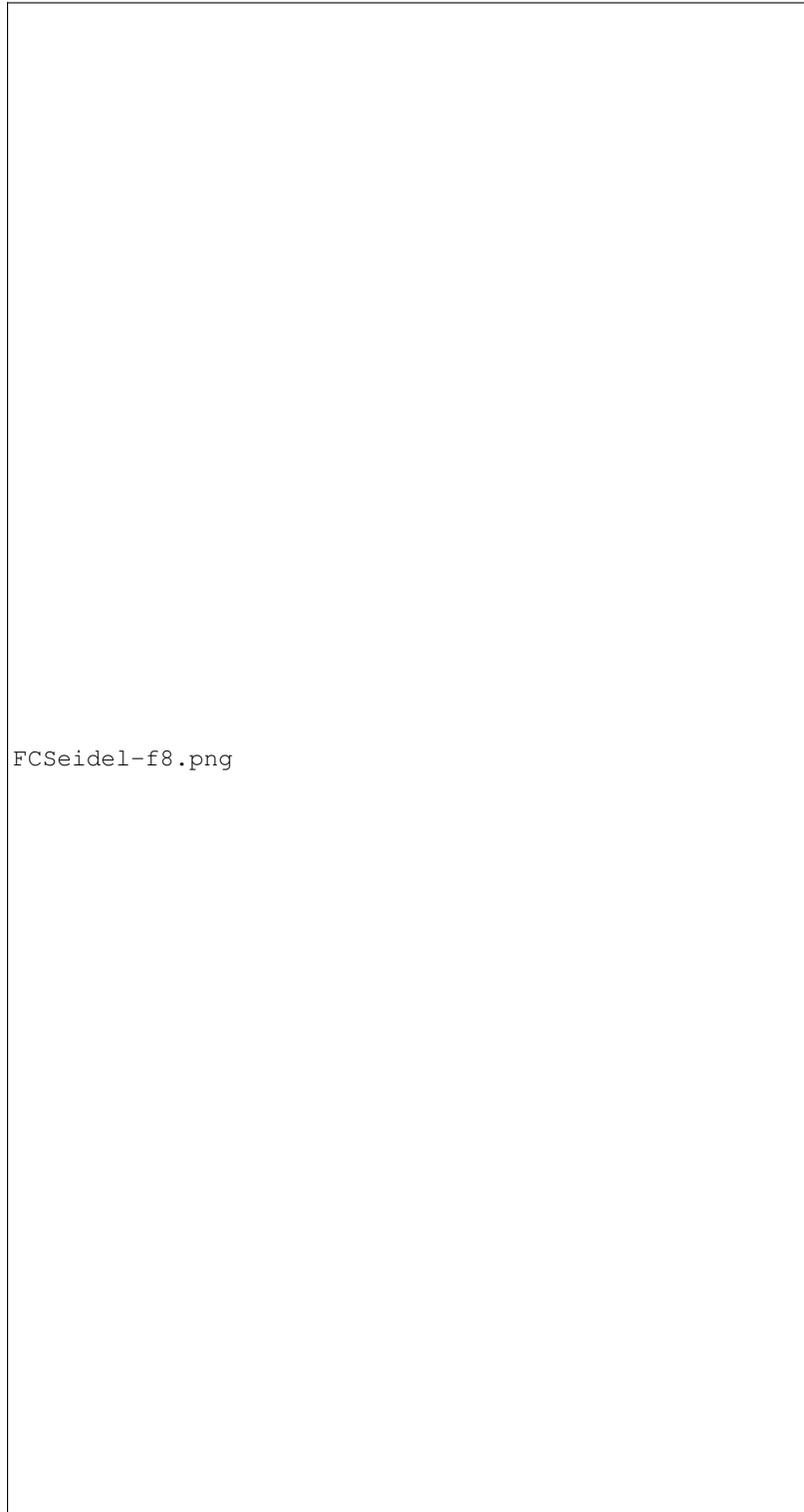


Figure 8. ~~Snow~~ Two-dimensional histogram of snow grain size with respect to terrain elevation (left) and aspect (right) in the Sierra Nevada in spring 2009.



Figure 9. Same as Fig. 8 but for the Rocky Mountains in spring 2011. Note: A rare retrieval artifact is found on 15 June where Eq. 4 has no unique solution within a snow grain size range of 540 to 570 μm causing a gap in the corresponding plots.

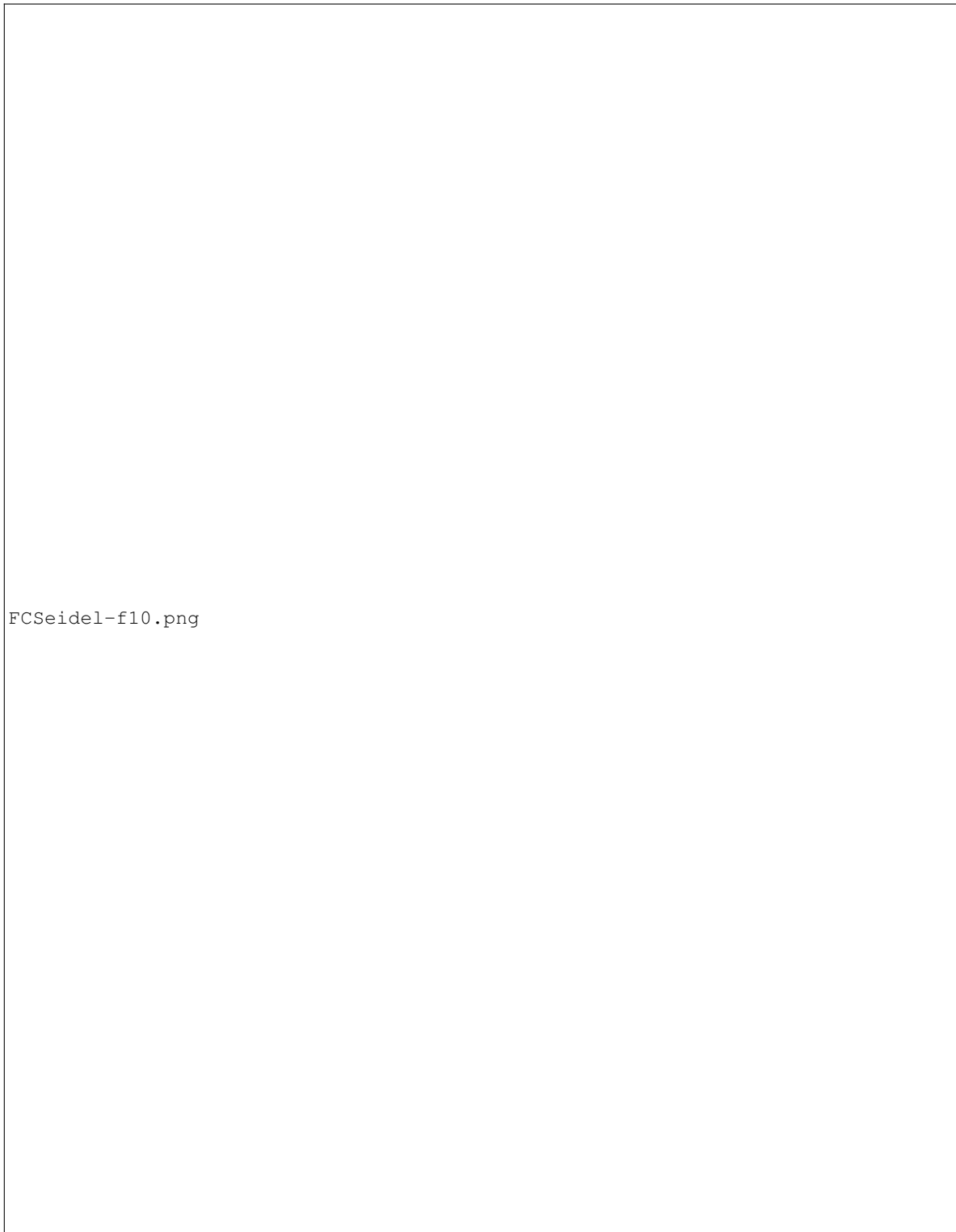


Figure 10. Snow albedo along a North–South (left), and West–East transect (right) through the middle of the observed Sierra Nevada area. The values are smoothed with a boxcar average of 30 pixels. The snow-free surface is shown in black.



Figure 11. Same as Fig. 10 but for the Rocky Mountains.



Figure 12. Snow albedo with respect to terrain elevation (left) and terrain aspect (right) in the Sierra Nevada in spring 2009.



FCSeidel-f13.png

Figure 13. Same as Fig. 12 but for the Rocky Mountains in spring 2011.



Figure 14. Radiative forcing of snow impurities with respect to terrain elevation (left) and aspect (right) in the Sierra Nevada in spring 2009.



Figure 15. Same as Fig. 14 but for the Rocky Mountains in spring 2011.